Active tectonics of the Turkish-Iranian Plateau

Alex Copley[1] and James Jackson[1]

Received 20 September 2005; revised 16 August 2006; accepted 22 September 2006; published 20 December 2006.

[1] This paper examines how active faulting in the Turkey-Iran-Caucasus region accommodates the Arabia-Eurasia collision and the velocity field observed by GPS. The overall shortening across the zone is, in general, spatially separated (''partitioned'') into right-lateral strike slip in the Turkish-Iranian Plateau and thrusting in the Greater Caucasus. A band of counterclockwise rotating NW-SE right-lateral strike-slip faults accommodates a NW-SE gradient in NE directed velocity (relative to Eurasia) between the Black and Caspian seas. A NNW-SSE band of previously unrecognized oblique normal faults is present on the Turkey-Iran border. We estimate the offsets on faults from geomorphological features and show that these offsets can be achieved in 5 ± 2 Ma at present rates. This implies a reorganization of deformation in the collision zone at that time, after the initial collision at ~12 Ma, probably in response to mantle-induced dynamic uplift. **Citation:** Copley, A., and J. Jackson (2006), Active tectonics of the Turkish-Iranian Plateau, *Tectonics*, *25*, TC6006, doi:10.1029/2005TC001906.

1. Introduction

[2] A central question in continental tectonics is how faulting in the seismogenic upper crust accommodates the velocity field that describes the overall characteristics of the deformation. Once that is understood, other questions related to the dynamics of the deformation, such as why the velocity field has the characteristics and distribution that are observed, can be properly posed. The region of eastern Turkey, northwest Iran, and the Caucasus has the highest elevation in western Asia, where the collision between Arabia and Eurasia is purely intracontinental, and is similar to the situation of the Pamir-Karakoram in the India-Eurasia collision. The subject of this paper is how the faulting achieves the velocity field in this key region of western Asia.

[3] The Turkish-Iranian Plateau (Figure 1) has an average elevation of approximately 2 km, and is composed of continental fragments accreted to the margin of Eurasia by the Late Cretaceous or early Tertiary, melanges, ophiolites, and a covering of volcanic rocks and Cenozoic sediments [e.g., *Sengör*, 1990]. The onset of the current purely intracontinental tectonics, marked by the cessation of marine sedimentation in eastern Anatolia, is thought to have occurred at about 12 Ma [*Dewey et al.*, 1986]. This is similar to the estimate of *McQuarrie et al.* [2003], who reconstruct the margins of Arabia and Eurasia and, using the motion of Arabia with respect to Eurasia deduced from seafloor magnetic anomalies and fracture zones, as well as the kinematics of the Red Sea, suggest that continent-continent collision started close to, but before, 10 Ma. It was in the Sarmatian (13.3–10.7 Ma) that the Paratethys sea became isolated, and the connection between its remnants in the Black Sea and Caspian Sea was severed by uplift in the area which is now the Turkish-Iranian Plateau [e.g., *Van Couvering and Miller*, 1971]. *McQuarrie et al.* [2003] also show that the Arabia-Eurasia convergence has been relatively constant at a rate of 20 to 30 mm yr^{-1} since 56 Ma (at ~33°N 50°E), a value similar to the GPS-derived rate at the same location. On the southern margin of the Turkish-Iranian Plateau (at 36°N, 43°E), geodetically determined poles of relative rotation [e.g., *McClusky et al.*, 2003] show that the convergence is around 17 mm yr^{-1} in the direction 345°. Seismic activity is widespread throughout the area (Figure 1; see auxiliary material for focal parameters of all the earthquakes mentioned in this paper).[1] Strike-slip faulting and normal faulting are generally dominant within the high plateau, while, with the exception of a small area in the SW part of the plateau, active shortening is confined to areas of lower elevation on the edge of the high ground. Since 6–8 Ma, the plateau has been a site of major volcanic activity, showing a number of different eruption styles (from shield volcanoes to stratovolcanoes) and chemistries (from mildly alkaline to calc-alkaline) [e.g., *Innocenti et al.*, 1976a, 1976b; *Pearce et al.*, 1990].

[4] *Jackson* [1992] noted that a spatial separation of subparallel thrusts and strike-slip faults, with orthogonal slip vectors (sometimes called ''strain partitioning'') appears to be occurring in the Turkish-Iranian Plateau and Caucasus. He used earthquake focal mechanisms and slip vectors (Figure 2b) to show that the eastern part of the Greater Caucasus accommodates NE-SW shortening perpendicular to the strike of the belt, with the remainder of the relative motion between the bounding plates being taken up by NW-SE right-lateral strike-slip faulting in the Turkish-Iranian Plateau. The GPS measurements of *McClusky et al.* [2000] confirmed the essential features of this strain partitioning, with velocities relative to Eurasia being directed slightly west of north to the south of the strike-slip faulting, and northeastward between the strike-slip faulting and the Greater Caucasus (Figure 2a).

[1]COMET, Department of Earth Sciences, University of Cambridge, Cambridge, UK.

0278-7407/06/2005TC001906

[1]Auxiliary materials are available at ftp://ftp.agu.org/apend/tc/2005tc001906.

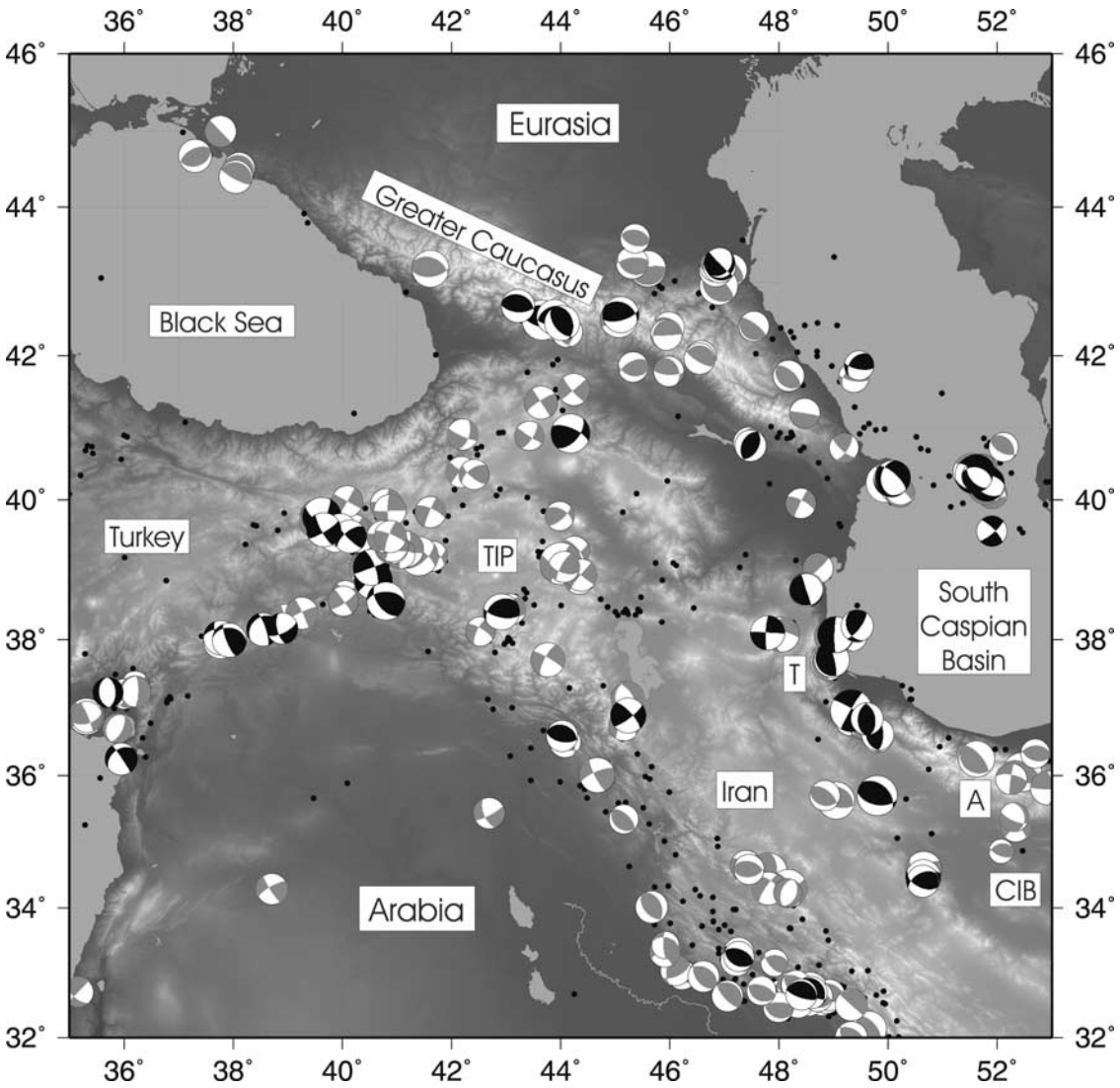

Figure 1. Seismicity of the Turkish-Iranian Plateau and surrounding areas. A, Alborz; CIB, Central Iranian Block; T, Talesh; TIP, Turkish-Iranian Plateau. Focal mechanisms for earthquakes of magnitude greater than 5.2 are from teleseismic waveform modeling (black) or from first motions and the CMT catalog (http://www.seismology.harvard.edu/CMTsearch.html) if the solutions are more than 70% double couple (gray). The percentage double couple is defined to be $\gamma = 100\{1 - [(2|\lambda_2| \times 1.5)/(|\lambda_1| + |\lambda_3|)]\}$, where λ_1, λ_2, and λ_3 are defined to be the maximum, intermediate, and minimum eigenvalues of the moment tensor, and is a measure of how well the moment tensor approximates the double couple source for the earthquake. See *Jackson et al.* [2002] for a fuller description. The band of normal faulting earthquakes across the central Caspian Sea are all deeper than 30 km [*Jackson et al.*, 2002]. All the other earthquakes on this plot are thought to have depths less than ~20 km. The black dots are epicenters from the *Engdahl et al.* [1998] catalog. See the auxiliary material for focal parameters of these earthquakes.

[5] However, since these studies, additional earthquake and GPS data have highlighted other features of the deformation in this area that require explanation. First, it is now clear that the entire eastern coast of the Black Sea is essentially part of Eurasia, with very little deformation occurring in the western Caucasus of Georgia (Figure 2a). A band of earthquakes associated with active NE-SW left-lateral faulting separates the southeastern Black Sea from the Turkish-Iranian Plateau (Figure 1) [*Philip et al.*, 1989; *Jackson*, 1992]. Second, the GPS data show a strong eastward increase in the northeastward velocities in the eastern part of the Turkish-Iranian Plateau (Figure 2a), and it is not obvious how this gradient is accommodated by faulting.

[6] We use geomorphological and seismological information, and the geodetically determined velocities of

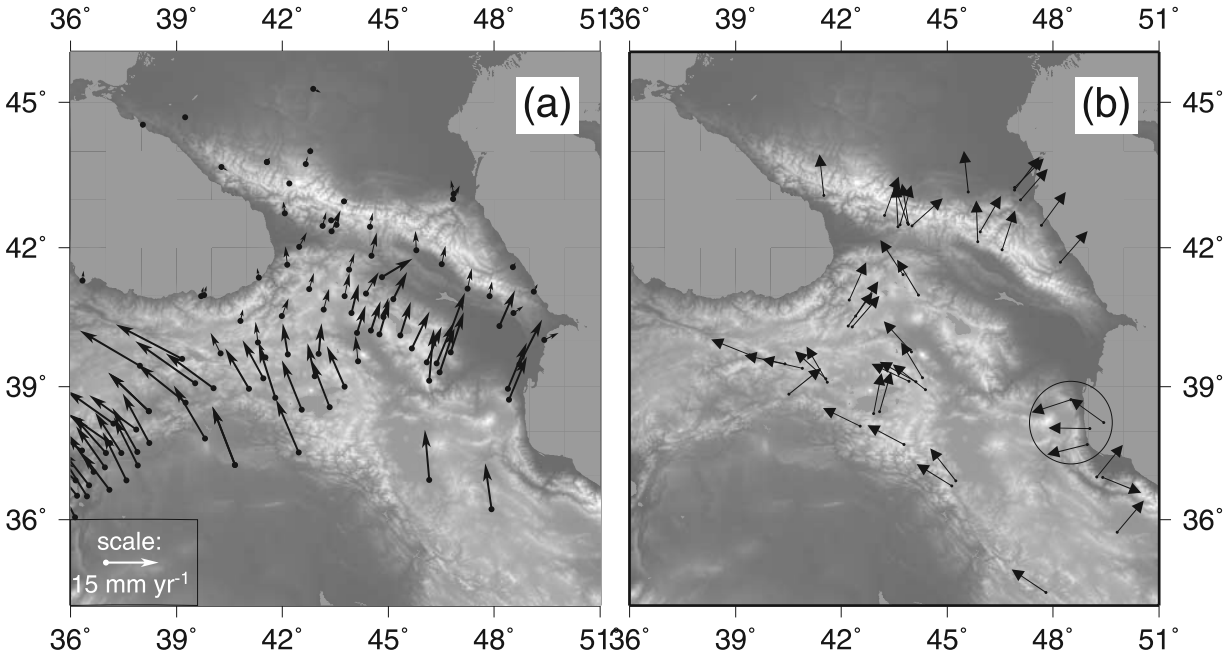

Figure 2. (a) Velocities relative to Eurasia, from the GPS data of *Reilinger et al.* [2006]. Error ellipses have been omitted. (b) Slip vectors for earthquakes in which the fault plane is known or can be inferred. The slip vectors show the motion of the southern side of the fault relative to the northern, except the E-W slip vectors on the eastern edge of the plateau (circled), which show the motion of the eastern side of the fault relative to the western.

Reilinger et al. [2006] (which include and update the results of *McClusky et al.* [2000] and *Vernant et al.* [2004a]) to examine the relations between the faulting and velocity field in this area, and to infer for how long the current regime of faulting has operated. We show later that right-lateral strike-slip faulting in the northern part of the plateau accommodates the motion between counterclockwise rotating crustal blocks, which are in turn accommodating a NW-to-SE gradient in northeastward velocities that is produced by an along-strike change in the rate of shortening in the Greater Caucasus. We present a new estimate for the motion of the South Caspian Basin relative to Eurasia, and a revised estimate for the total displacement on the Main Recent Fault, on the northeast edge of the Zagros, which may reconcile GPS and long-term estimates for the slip rate. We also suggest that at current rates of motion the faults in the area could account for the total displacements observed in 5 ± 2 Ma and that there was a change in the nature of the collision zone at this time.

2. Characteristics of the Active Faulting

[7] The locations, and some details of the history and kinematics of the active faults in the area are known from the work of *Toksoz et al.* [1977], *Saroglu and Guner* [1979], *Saroglu and Hempton* [1982], *Ambraseys* [1988], *Barka and Kadinsky-Cade* [1988], *Philip et al.* [1989], *Saroglu et al.* [1992a], *Karakhanian* [1993], *Karakhanian et al.* [1993], *Trifonov et al.* [1994], *Berberian* [1997], *Bozkurt* [2001], *Philip et al.* [2001], *Guidoboni et al.* [2003], and *Karakhanian et al.* [2004], as well as from focal mechanisms of earthquakes and our own field- and remote-sensing-based observations. The main features of the active fault patterns are described below, and then combined in section 3 into a coherent kinematic description of the overall deformation.

2.1. Right-Lateral Strike-Slip Faulting in Eastern Turkey and Northwest Iran

[8] In the southern portions of the Turkish-Iranian Plateau, there are numerous subparallel NW-SE right-lateral strike-slip faults (Figure 3), which are part of the system of strain partitioning described by *Jackson* [1992]. The slip vector of the 1976 M_w7.1 Chaldiran earthquake (which occurred on the Chaldiran fault, Figure 3) was purely strike slip (see the auxiliary material) and suggests that the slip vector on the faults in this region is between 290° and 300° (throughout this paper the azimuth quoted for the slip vector represents the direction of motion of the southern side of the fault relative to the northern side). The available GPS data show that most of the strike-slip motion is accommodated in an area which in places is up to 80 km wide (Figure 3) north of Lake Van, with a shear across the area of 8 ± 2 mm yr^{-1} (Figure 4a). This is similar to the estimate of *Reilinger et al.* [2006], who use a block model to estimate a shear in this area of 12 ± 1 or 10 ± 1 mm yr^{-1}, depending on which faults are included in their model. We refer to this band of distributed right-lateral faulting as the Van shear zone. It extends from

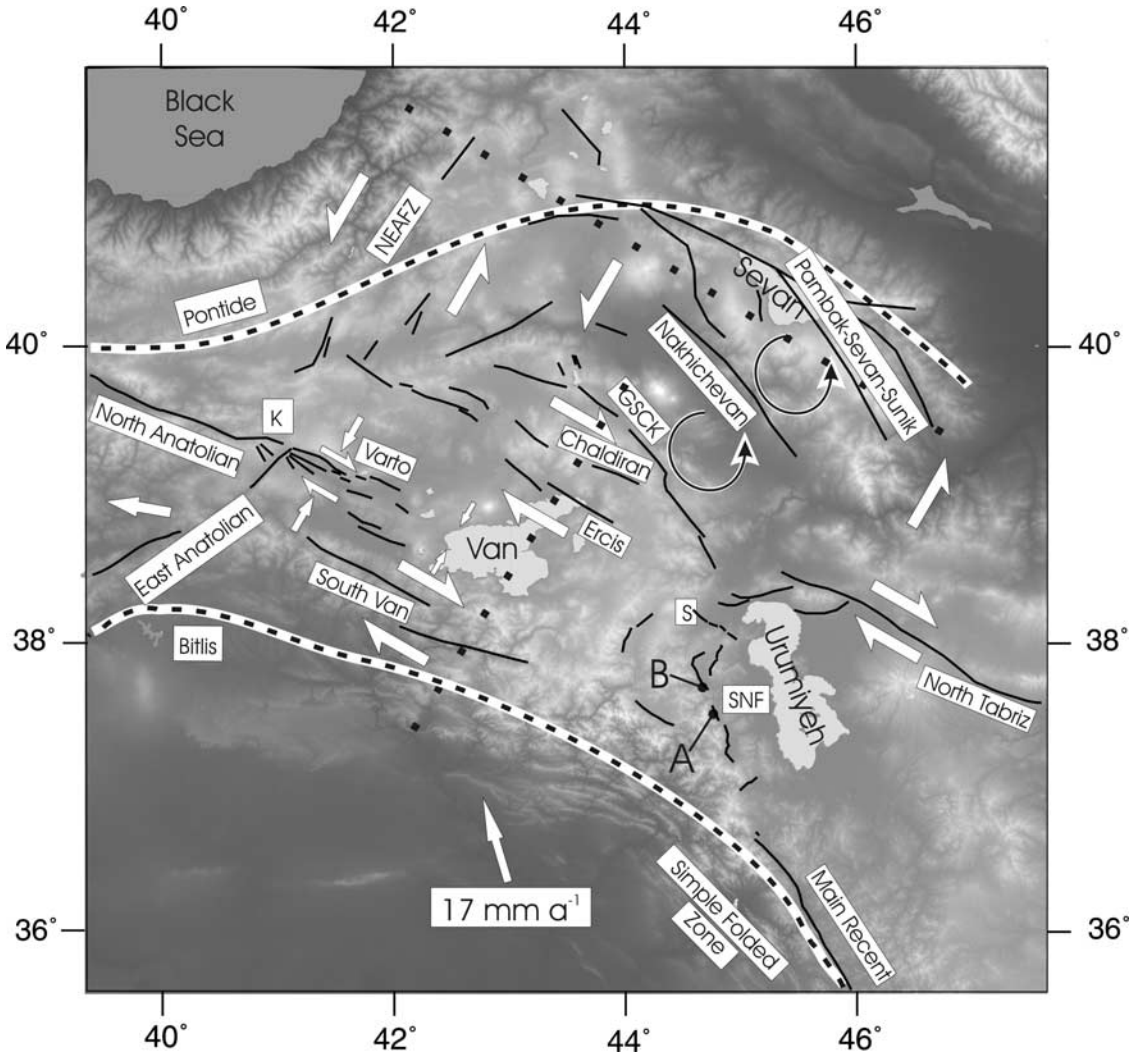

Figure 3. Major faults in the Turkish-Iranian Plateau, from the references given in the text and our own observations. The faults are labeled, with the ''fault'' suffix removed for clarity. GSCK, Gailatu-Siah Chesmeh-Khoy fault; K, Karliova triple junction; NEAFZ, Northeast Anatolian fault zone; SNF, Serow normal faults; S, Salmas fault. Also labeled are lakes Sevan, Urumiyeh, and Van. Open white arrows signify shortening. All E-W to NW-SE faults are right lateral, while NE-SW ones are left lateral. The NE-SW and NW-SE lines of black squares show the position of the velocity profiles in Figures 4a and 4b, respectively. A and B show the locations of the exposed fault planes on the Serow normal faults shown in Figures 5a and 5b. The thin black dotted lines show the approximate locations of the Pontide and Bitlis sutures.

the Varto fault (Figure 3) near the Karliova triple junction (K in Figure 3) in the west to the eastern end of the North Tabriz fault in the east, which is close to the western margin of the Caspian Sea. Right-lateral shear is also present south of Lake Van, with a slower rate of $2-3 \pm 2$ mm yr^{-1} (Figure 4a). To the west and east of this area, right-lateral strike-slip deformation is not distributed, but concentrated onto major faults (the North Anatolian and Main Recent faults, respectively).

[9] Right-lateral strike-slip faulting is also present within the plateau NE of the Chaldiran fault, on the Gailatu-Siah Chesmeh-Khoy (GSCK), Nakhichevan, and Pambak-Sevan-Sunik faults (Figure 3). The slip rates on these faults are probably lower than those closer to Lake Van. For example, *Philip et al.* [2001] estimate $2-4$ mm yr^{-1} on the Pambak-Sevan-Sunik fault from offset rivers. Recent earthquakes occurred on these faults in 1968, 1970, and 2004 (near the Gailatu-Siah Chesmeh-Khoy (GSCK) fault) and 1988 (the Spitak earthquake, near the Pambak-Sevan-Sunik fault). With the exception of the NW end of the Pambak-Sevan-Sunik fault, these faults have a more N-S trending strike than those in the main Van shear zone. In addition, the NE directed GPS velocities in the area of these faults show a major gradient increasing to the SE (Figures 2a

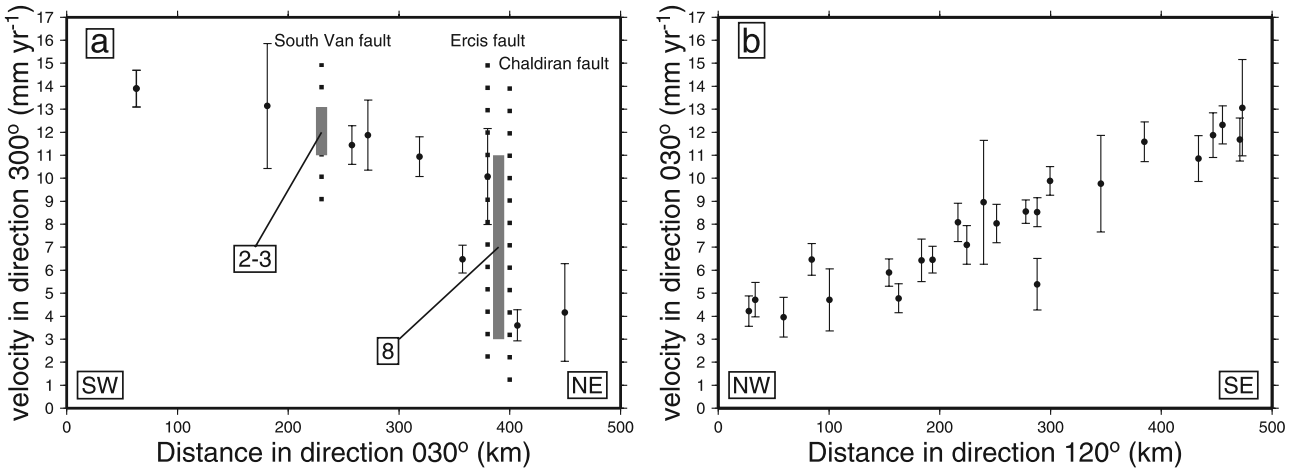

Figure 4. (a) Components of velocity in the direction 300°, parallel to the Chaldiran, Ercis, and South Van faults along the line of the SW-NE black dotted line in Figure 3, from the GPS data of *Reilinger et al.* [2006]. The locations of the faults (shown by the vertical dotted lines) are known from seismological and geomorphological evidence. The slip rate for the South Van fault is around 2–3 mm yr^{-1}, and that for the Chaldiran and Ercis faults combined is around 8 mm yr^{-1}, as shown by the thick vertical solid lines. (b) Components of velocity in the direction 030° in the northern Turkish-Iranian Plateau along the line of the NW-SE black dotted line in Figure 3, showing the increase in northeastward velocity to the SE.

and 4b). We will return to the kinematics of this faulting in section 3.3.

2.2. Oblique Normal Faulting in Northwest Iran

[10] There is evidence for previously unrecognized oblique normal faulting along the border between northwest Iran and eastern Turkey, hereinafter referred to as the Serow normal faults (SNF in Figure 3). The morphological expression of the faults is characterized by abrupt range fronts displaying triangular facets, "wine-glass canyons," and sedimentary basins on the hanging wall side. Back-tilted Neogene sediments dipping ~15°W were visible in the footwall of the faults. The motion on these faults is a mixture of normal and right-lateral strike slip. A slip vector between 290° and 300° was measured on an exposed fault plane (Figure 5a) at locality A in Figure 3. This direction is parallel to the slip vector for the right-lateral strike-slip faults near Lake Van, such as the Chaldiran and Ercis faults, and similar to the slip vector of approximately 300°–310° suggested by *Talebian and Jackson* [2002] for the Main Recent Fault. We will return to the possible

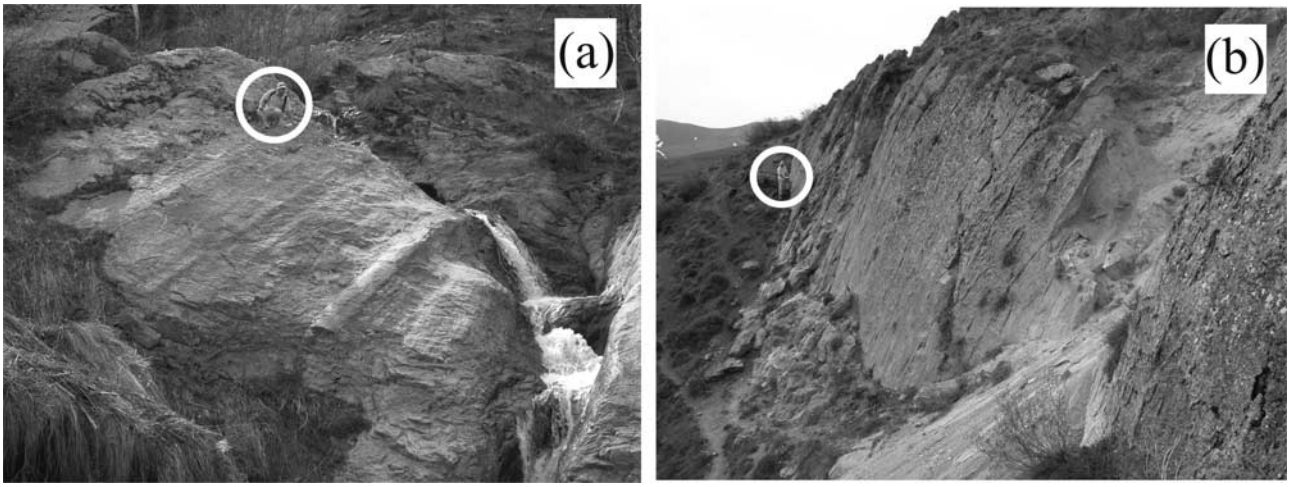

Figure 5. Exposed fault planes on the Serow normal fault system. Note the people (circled) for scale. (a) A fault plane near the village of Sulak (37.492°N, 44.761°E). Corrugations on the fault plane show the slip vector to be between 290° and 300°. View is to the west. (b) An exposed fault plane near the village of Gol Shukhein (37.684°N, 44.666°E). View is to the south.

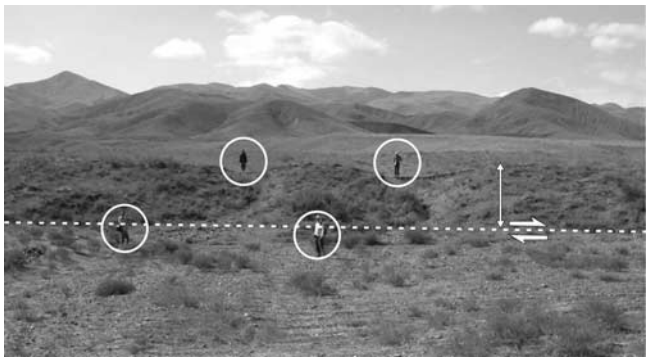

Figure 6. View looking southwest at 38.121°N, 44.754°E of the scarp produced by the 1930 Salmas earthquake. The dashed line runs along the base of the coseismic scarp. The four people (circled) stand in watercourses that were offset vertically by ~4 m (double arrow) and right laterally by ~4 m during the 1930 earthquake.

reasons for this in section 3.1. Another fault plane at locality B in Figure 3 shows a slip vector of 250° to 260° (Figure 5b), with the faulting being almost pure normal faulting. However, the geological offsets nearby (section 4.1.5) indicate that the overall slip vector near this fault plane is similar to that in Figure 5a (i.e., 290°–300°), suggesting that there must also be a strike-slip fault present in this part of the fault system, probably hidden in the hanging wall basin of the normal faults, and that the strain has been partitioned into almost pure normal faulting and strike-slip faulting.

[11] The 1930 Salmas earthquake, which occurred on the fault marked S in Figure 3, produced spectacular surface faulting (Figure 6) with a NW-SE strike, and involved almost equal components of normal and right-lateral slip [*Tchalenko and Berberian*, 1974; *Berberian and Tchalenko*, 1976]. This implies a slip vector between E-W and NW-SE, which is similar to that measured for the other normal faults discussed here, so it is likely that the Salmas fault helps accommodate the same motion as the Serow normal faults.

2.3. Left-Lateral Strike-Slip Faulting in Eastern Turkey

[12] Left-lateral strike-slip faulting trending NE-SW occurs NE of the North Anatolian Fault in a zone near the eastern margin of the Black Sea. Ground ruptures of this orientation were observed after the 1983 Narman earthquake (at 40.39°N, 42.18°E [*Barka et al.*, 1985; *Ambraseys*, 1988]), and the geodetic data of *Reilinger et al.* [2006] confirm the overall sense of motion across this zone (Figure 4b). This area is SW of, and along strike from, the Borjomi-Kazbeg left-lateral strike-slip fault zone described by *Philip et al.* [1989] and is sometimes called the northeast Anatolian fault zone. Seismic activity in the area (Figure 1) is diffuse, showing that there is more than one fault present. These faults have little visible expression in remote sensing data (both topographic data and satellite imagery) due to the nature of the landscape, which is composed of deeply eroded volcanics and sediments. GPS data [*Reilinger et al.*, 2006] show that the cumulative slip rate for these faults is around 2 ± 2 mm yr^{-1}.

2.4. Thrust Faulting in the Greater Caucasus

[13] The Greater Caucasus mountain range forms the northern edge of the collision zone (Figure 1). Focal mechanisms (e.g., *Fuenzalida et al.* [1997] and the Harvard centroid moment tensor (CMT) catalog) show this to be an area of active thrusting, with shallow-dipping nodal planes in focal mechanisms inclined toward the range on both its northern and southern margins. Earthquakes are more common in the east of the range than the west (Figure 1), and GPS data [*Reilinger et al.*, 2006] show that the overall rate of shortening is also higher in the east (Figures 2a and 4b).

2.5. The Talesh

[14] The Talesh mountains are situated on the western margin of the South Caspian Basin (Figure 1). Focal mechanisms show that the South Caspian is underthrusting the Turkish-Iranian Plateau in this area on low-angle faults that reach depths of approximately 30 km [*Priestley et al.*, 1994; *Jackson et al.*, 2002]. It is unclear whether the strike-slip earthquakes near 38°N 48°E occur on approximately E-W right-lateral strike-slip faults (similar to those described farther west) at the SE edge of the plateau or on N-S left-lateral strike-slip faults along the margin of the South Caspian.

2.6. Main Recent Fault

[15] Throughout the length of the Zagros mountains, to the SE of the Turkish-Iranian Plateau, considerable shortening (e.g., 6.5 ± 2 mm yr^{-1}, *Vernant et al.* [2004a]) takes place on the southern margin of the Arabia-Eurasia collision zone. In the NW Zagros, strain partitioning exists, with NE-SW shortening along the SW front of the range (the Simple Folded Zone, Figure 3), and NW-SE right-lateral strike slip on the Main Recent Fault to the NE (Figures 1 and 3) [*Talebian and Jackson* [2004]. There is little seismic evidence for active shortening on the southern margin of the Turkish-Iranian Plateau itself (Figure 1), and the main locus of shortening in the area NW of the Zagros is in the Greater Caucasus. As a clear morphological and structural feature, the Main Recent Fault ends in the NW near 36.7°N, 45.1°E, where seismicity suggests that shortening on the southern margin of the collision zone almost dies out (Figure 1).

[16] Near the NW end of the Main Recent Fault are two pull-apart basins (Figure 7). An earthquake in 1970 occurred near these basins, with a mechanism showing oblique right-lateral and normal motion. Figure 8 shows the range front at 45.14°E 36.61°N (location A in Figure 7), with the triangular facets characteristic of a normal component of motion. Figure 9 shows an exposure of a fault plane nearby at 36.578°N 45.180°E (location B in Figure 7), with weak remnant corrugations that probably indicate a slip vector of between 280° and 290°. From the amount of motion on the fault required to "close" the pull-apart

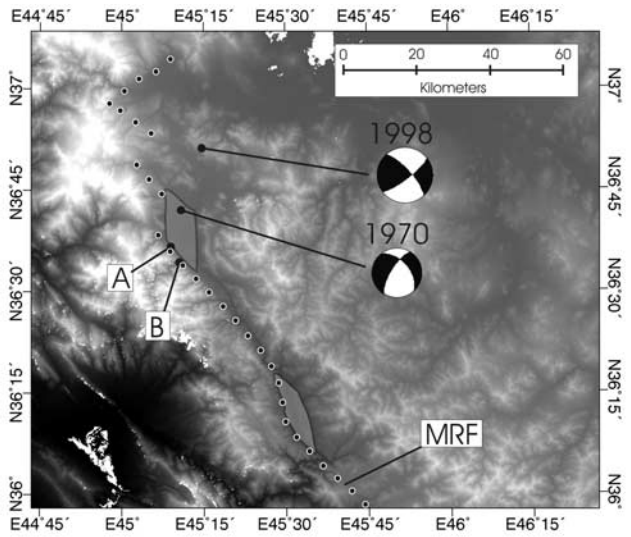

Figure 7. Topography and faulting (dotted black lines) at the northern end of the Main Recent fault (MRF) showing the presence of two pull-apart basins (shaded in gray). These basins cease to exist if 10–15 km of right-lateral motion is removed along the line of the fault. A shows the position of the range front shown in Figure 8, and B shows the position of the fault plane in Figure 9.

Figure 9. An exposure of a weathered fault plane at 36.578°N, 45.180°E (B in Figure 7) on the fault in Figure 8. View is to the SW. Possible remnant corrugations indicate a combination of right-lateral and normal faulting (with a direction shown by the arrow and a slip vector azimuth between 280° and 290°).

basins, the total offset on the Main Recent Fault at this northwestern end can be estimated to be 10–15 km. If the onset of slip on the Main Recent Fault was at 3–5 Ma as suggested by *Talebian and Jackson* [2002], then the calculated slip rate for this part of it, using the geomorphologically derived total displacement of 10–15 km, is 2–5 mm yr^{-1}. This value falls within the range of slip rates suggested by *Vernant et al.* [2004a] (3 ± 2 mm yr^{-1}) and *Walpersdorf et al.* [2006] (4–6 mm yr^{-1}) based on GPS observations, and also by *Authemayou* [2006] (5–7 mm yr^{-1}) based on quaternary geological offsets. Farther south, *Talebian and Jackson* [2002] estimate a total displacement on the Main Recent Fault of 50 km, which would require a higher long-term slip rate of 10–17 mm yr^{-1} if it accumulated over 3–5 Ma. We return to this issue in section 4.3.

3. Faulting and the Velocity Field

3.1. Oblique Normal Faulting in Northwest Iran

[17] The pole of rotation that describes the relative motion between Arabia and Eurasia is situated in north Africa, at approximately 18°N 27°E [*McClusky et al.*, 2003]. This is close enough to the Turkish-Iranian Plateau for significant variations in the magnitude and direction of the overall Arabia-Eurasia motion to exist along the length of the area being considered here (i.e., a velocity relative to Eurasia of ~16 mm yr^{-1} along 340° at 37°N 41°E compared with ~18 mm yr^{-1} along 354° at 33°N, 46°E). The right-lateral strike-slip faults which accommodate the component of the overall motion that is not taken up by shortening in the Caucasus have the same strike along their

Figure 8. View looking SW of the range front (A in Figure 7) formed by the fault bounding the pull-apart basin near Piranshahr, at the NW end of the Main Recent fault (45.14°E, 36.61°N). Note the abrupt edge to the topography and the triangular facets.

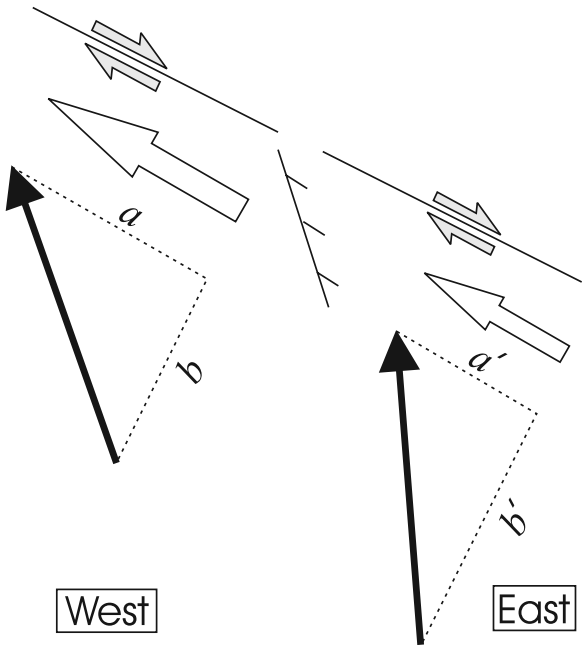

Figure 10. A cartoon (not to scale) to illustrate a possible origin for the oblique normal faults in northwest Iran. The overall Arabia-Eurasia motion (thick black arrows) changes along the WNW-ESE strike of the belt. Therefore the component of the motion which is being expressed as right-lateral strike-slip faulting (lines a and a') changes along the belt. If the northern boundary of the faults is effectively undeforming, then there is a difference in fault-parallel velocities south of the faults (white arrows) which the normal faults can accommodate. Note that the amount of shortening to be accommodated in the Greater Caucasus (lines b and b') is higher in the east than the west.

entire length from the Karliova triple junction (K in Figure 3) to the eastern end of the North Tabriz fault. Because the overall relative motion that is accommodated varies along the belt, the strike-slip component should change along the belt, increasing in rate to the west. The role of the oblique normal faults in the Serow fault system (SNF) may be to accommodate this change in slip rate along the strike-slip faults (Figure 10), which would explain the similarity of the slip vectors for the two types of faulting. If the normal faults are accommodating all of the gradient in strain along the strike-slip system, then the pole of Arabia-Eurasia motion of *McClusky et al.* [2003] would suggest a slip rate for the normal faults of around 1.6 mm yr^{-1}. The GPS stations at 36.9°N 46.2°E and 38.5°N 43.3°E [*Reilinger et al.*, 2006] can be used to give a very rough estimate of the slip rate on the normal faults if they accommodate all of the motion between the two stations that is parallel to the slip vector. This estimate is $\sim$3 mm yr^{-1}. Given the uncertainties in the GPS measurements and the precise position of the Arabia-Eurasia pole, these values are in reasonable agreement. A test of this hypothesis would be to compare the slip rates on the strike-slip faults west of the normal faults with that of the North Tabriz fault, which is to the east and should be moving more slowly. At present, however, these slip rates are not known with a high enough level of accuracy for such a comparison to be meaningful, given the small differences in slip rate expected.

[18] *Talebian and Jackson* [2002] suggested that the slip vector for the Main Recent Fault near 34°N is approximately 300°–310°. The Serow normal faults have a similar slip vector of 290°–300° (Figure 5). Thus, although there is no throughgoing fault between the Main Recent Fault and the Serow normal faults, it is possible that some of the motion on the normal faults is due to a continuation to the NW of the motion on the Main Recent Fault, thereby "linking" the Main Recent Fault with right-lateral strike-slip faults near Lake Van. The relative importance of this alternative explanation for the existence of the normal faults is not clear. They may well accommodate both possible causes of motion.

3.2. Left-Lateral Strike-Slip Faulting in Eastern Turkey

[19] The left-lateral strike-slip faulting along the eastern margin of the Black Sea is present because the Black Sea is essentially stationary with respect to Eurasia [*McClusky et al.*, 2000]. South of the Black Sea, the relative motion of Arabia and Eurasia is accommodated by westward motion of central Anatolia [e.g., *McKenzie*, 1970; *McClusky et al.*, 2000], but east of the Black Sea a major component of the Arabia-Eurasia motion is expressed as shortening in the Greater Caucasus. Thus between the latitudes of 40° and 42°N there is a velocity difference between the Black Sea and the Turkish-Iranian Plateau area, which is moving toward the Greater Caucasus (Figure 2a). This difference is accommodated by left-lateral shear between the two areas.

3.3. Right-Lateral Strike-Slip Faulting in the NE Part of the Plateau

[20] In addition to the right-lateral strike-slip faulting of the Van shear zone (section 2.1), there is a series of right-lateral faults with more N-S oriented strikes and lower slip rates in the northeastern plateau, in particular the Galiatu-Siah Chesmeh-Khoy (GSCK in Figure 3), Nakhichevan, and Pambak-Sevan-Sunik faults. These faults must accommodate the variation in shortening rate along strike in the Greater Caucasus, which is higher in the east than the west. This along-strike variation in the Caucasus arises partly because the rate and azimuth of convergence between Arabia and Eurasia changes along the length of the collision zone, leading to greater shortening in the east (Figure 10), and partly because there is a southern zone of shortening between Varto and Lake Van which dies out to the east (Figure 3). This southern zone of shortening east of the Karliova triple junction is manifested by faults with a combination of right-lateral and shortening motion, such as the 1966 Varto earthquake fault [*Ambraseys and Zátopek*, 1968; *McKenzie*, 1972], and the thrust faults between Varto and Lake Van described by *Saroglu and Hempton* [1982]. The gradient in shortening rate along the Greater Caucasus produces a

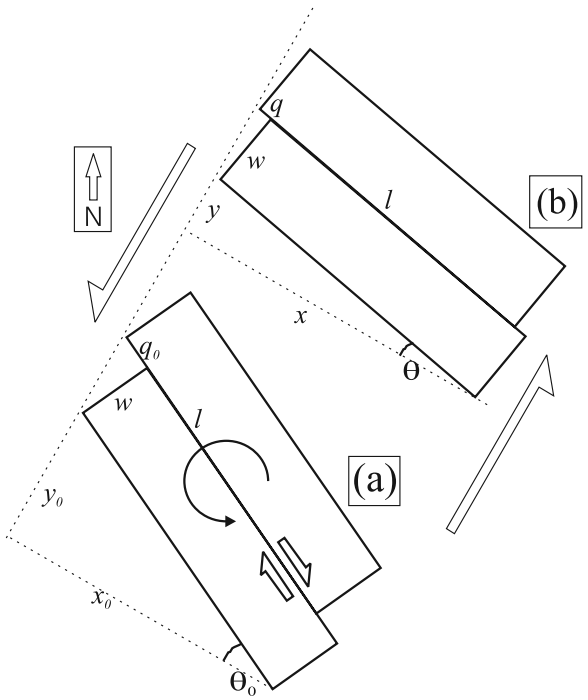

Figure 11. Idealized geometry of the counterclockwise rotating blocks bounded by right-lateral strike-slip faults in the NE Turkish-Iranian Plateau, discussed in the text. As time advances the blocks rotate from the position shown in Figure 11a to that in Figure 11b. Their motion accommodates a NE-SW right-lateral shear.

gradient in the NE directed velocities measured in the northern part of the Turkish-Iranian Plateau (Figure 4b) which must somehow be accommodated by the NW-SE striking right-lateral strike-slip faults. We suggest this is achieved by the faults rotating counterclockwise, illustrated schematically in Figure 11. It can be seen from Figure 11 that $y = l \sin \theta$. Therefore δy, the NE motion of one end of a block relative to the other, can be calculated as $\delta y = l \sin \theta_0 - l \sin \theta$. The slip that has occurred on the faults during rotation between θ_0 and θ is $s = q - q_0 = w \tan \theta_0 - w \tan \theta$. Eliminating θ_0 gives $\delta y = l \sin \{\tan^{-1} [(s + w \tan\theta)/w]\} - l \sin \theta$, which allows us to relate the relative motion of the ends of the blocks to the slip on the faults. If the blocks bounded by the Gailatu-Siah Chesmeh-Khoy, Nakhichevan, and Pambak-Sevan-Sunik faults are taken to measure 300 km (l) by 75 km (w) (see Figure 3), θ is 20°, and the left-lateral shear across the area on NE-SW planes is taken to be 8 mm yr^{-1} (from the GPS data in Figures 2a and 4b), then the predicted right-lateral slip rate on each of the faults is 2.4 mm yr^{-1}. This is close to the estimates of the slip rate on the Pambak-Sevan-Sunik Fault of 3–4 mm yr^{-1} given by *Trifonov et al.* [1994] and 2.24 ± 1 mm yr^{-1} given by *Philip et al.* [2001] (they give an estimate of 0.53 ± 0.04 mm yr^{-1} on another part of the fault, which may be lower because the fault appears to have more than one branch in that area). In section 4.1.2, we estimate the total displacement the Pambak-Sevan-Sunik fault to be 12 km, which would require a total counterclockwise rotation of about 8°. If this occurred over 5 ± 2 Ma, as we suggest in section 4.1, the rotation rate is in the range 1.1–2.7° Myr^{-1}.

[21] The analysis above is simplistic but shows that right-lateral slip with counterclockwise rotation on the Pambak-Sevan-Sunik, Nakhichevan, and Gailatu-Siah Chesmeh-Khoy faults can accommodate the gradient in NE-SW velocities seen in the GPS data. The analysis assumes that there is only strike-slip faulting between the blocks and that surface area is preserved. This may not be correct for some of the Pambak-Sevan-Sunik fault (PSS), which is known to have a dip-slip component in places [*Philip et al.*, 2001]. In particular, between 43.75°E and 45.25°E the fault has a more east-west strike than farther east (Figure 3), where it is parallel to the Nakhichevan and Gailatu-Siah Chesmeh-Khoy faults. It is in this western part that there is a significant topographic expression on the Pambak-Sevan-Sunik fault, close to where the Spitak earthquake occurred in 1988. That earthquake, although not on the main Pambak-Sevan-Sunik fault, had an oblique right-lateral and reverse slip vector, in the direction 318° [*Pacheco et al.*, 1989]. The reverse component is expected if the slip vector remains the same as the pure strike slip assumed in the eastern part of the NW-SE fault system. The lack of topographic expression on both the Nakhichevan and Gailatu-Siah Chesmeh-Khoy faults, as well as earthquake focal mechanisms on the latter, suggest that their motion is indeed purely strike slip in nature. Furthermore, the slip vector for the Spitak earthquake (318°) is similar to that for the 1968 (329°) and 2004 (318°) earthquakes which occurred on the Gailatu-Siah Chesmeh-Khoy fault (*McKenzie* [1972] and Harvard CMT catalog). Thus, though simplistic, the basic assumptions regarding the geometry and kinematics of the rotating blocks involved in the analysis of Figure 11 seem reasonable. *Reilinger et al.* [2006] reached a similar conclusion, namely, that counterclockwise rotations are occurring in this area. Their suggestion was based on the use of GPS velocities to create a block model for the tectonics of the area, and differs from ours by considering the area as one rigid block, so not including the Gailatu-Siah Chesmeh-Khoy or Nakhichevan faults in their model, and not including the Pambak-Sevan-Sunik fault in their preferred solution.

[22] To summarize, we suggest that the Gailatu-Siah Chesmeh-Khoy (GSCK), Nakhichevan and Pambak-Sevan-Sunik faults rotate counterclockwise and accommodate the NW-SE gradient in northeastward velocity in the northern part of the plateau. This is in contrast to the right-lateral strike-slip farther south (e.g., the Chaldiran and Ercis faults) which accommodate the belt-parallel component of the relative plate motion [*Jackson*, 1992].

3.4. Motion of the South Caspian

[23] *Jackson et al.* [2002] suggest that the South Caspian is moving NW with respect to Eurasia. Using recently published information, it is possible to revise the velocity triangle analysis that *Jackson et al.* [2002] used to estimate the motion of the South Caspian (Figure 12).

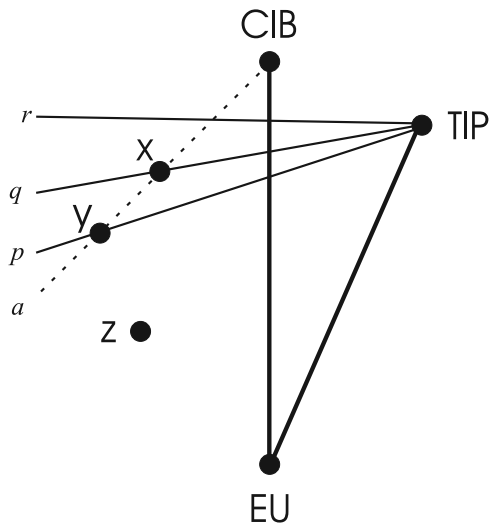

Figure 12. Construction of velocity triangles (not to scale) to show the motion between Eurasia (EU), the eastern Turkish-Iranian Plateau (TIP), the Central Iranian Block (CIB) and the South Caspian (x, y and z). See text for details.

[24] The motion of the eastern edge of the Turkish-Iranian Plateau relative to Eurasia is given by the GPS data of *Reilinger et al.* [2006] (Figure 2a), and is 13.6 mm yr^{-1} in the direction 024° (line EU-TIP in Figure 12). The pole of relative rotation for the Central Iranian Block (CIB) relative to Eurasia of *Vernant et al.* [2004a] is used to calculate the velocity relative to Eurasia of the area just south of the Alborz mountains (which accommodate the motion between the Central Iranian Block and the South Caspian, Figure 1). The direction (but not the rate) of motion of the South Caspian Basin with respect to the eastern edge of the Turkish-Iranian Plateau can be estimated from the slip vectors of thrust earthquakes in the Talesh (Figures 1 and 2b). Four thrust faulting earthquakes in, and offshore of, the eastern edge of the plateau (Table 1) have well constrained slip vectors that average 271° and give the direction of line *r* in Figure 12. If the 1981 event (c in Table 1) is discounted, as it is relatively small, is offshore, and has a noticeably different slip vector from the others, then the average is 260° (direction of line *q*). *Vernant et al.* [2004b] suggest that the South Caspian moves northwest at 6 ± 2 mm yr^{-1} with respect to Eurasia, based on the motion of a single GPS site on the Caspian shoreline. If this were the case, then the South Caspian Basin would plot at the point marked Z in Figure 12. This position, relative to TIP, would involve a significant amount of N-S right-lateral shear between the South Caspian and the Turkish-Iranian Plateau for which we see no evidence in geomorphological, geodetic, or seismological information. Geological reconstructions by *Allen et al.* [2003] estimated the total approximately E-W left-lateral slip in the Central Alborz (which accommodates the motion between the South Caspian and the Central Iranian Block) to be 30–35 km, with a total approximately N-S shortening at the same longitude of approximately 30 km. If the current tectonics of the Alborz mirror this pattern and the amounts of E-W left-lateral slip and N-S shortening are approximately equal, then the velocity of the South Caspian relative to the Central Iranian Block should plot in the direction of the dashed line *a*. Thus the motion of the South Caspian Basin should be represented by the point intersection between the dashed line *a* (South Caspian relative to the Central Iranian Block) and the various alternative lines r,q,p (South Caspian relative to the Turkish-Iranian Plateau). One possibility for the motion of the South Caspian is given by point x, indicating about 4.5 mm yr^{-1} of both N-S shortening and E-W left-lateral strike slip in the Alborz (x-CIB), and a motion of the South Caspian relative to Eurasia of ~11.5 mm yr^{-1} in a direction of ~340° (x-EU). If we use only the two similar and more southerly oriented slip vectors of the 1978 (a) and 1998 (d) earthquakes in Table 1 for the deformation between the Turkish-Iranian Plateau and the South Caspian (line *p*), then the estimates change to ~5.5 mm yr^{-1} of shortening and strike slip in the Alborz (line y-CIB) and 11 mm yr^{-1} of South Caspian-Eurasia motion in the direction 330° (y-EU). The velocity estimates in this section should be taken to have errors of at least ±2 mm yr^{-1}. *Vernant et al.* [2004b] use GPS to suggest 5 ± 2 mm yr^{-1} shortening and 4 ± 2 mm yr^{-1} strike-slip motion in the central Alborz. These values fall within our range of estimates. Our estimate of South Caspian motion predicts around 10–11.5 mm yr^{-1} shortening between the South Caspian and the eastern edge of the Turkish-Iranian Plateau (i.e., in the Talesh).

[25] *Jackson et al.* [2002] suggested rates of motion of the South Caspian of 7–10 mm yr^{-1} in a direction north of 300° with respect to Eurasia and 10–15 mm yr^{-1} in the direction 210° with respect to central Iran (see Table 2 for a comparison of estimates of South Caspian motion). The differences in our results stem from the alternative values used for the Central Iran-Eurasia motion, for which *Jackson*

Table 1. Details of Earthquakes on the Eastern Edge of the Turkish-Iranian Plateau Whose Mechanisms Are Constrained by Waveform Modeling[a]

	Year	Longitude	Latitude	M_w	z	Strike	Dip	Rake	Slip Vector	Reference
a	1978	48.97	37.71	6.12	21	141	12	65	256	P
b	1980	49.04	38.07	6.34	15	027	6	−63	271	P
c	1981	49.43	38.20	5.52	20	154	35	32	306	P
d	1998	48.50	38.71	5.69	27	72	8	0	252	J

[a]P are from *Priestley et al.* [1994]; J are from *Jackson et al.* [2002]; z is the centroid depth in km.

Table 2. Motion of the South Caspian Basin Relative to Eurasia and the Central Iranian Block[a]

Source	SCB-EU		SCB-CIB	
	Rate, mm yr^{-1}	Direction	Rate, mm yr^{-1}	Direction
This paper	~11 ± 2	330°–340°	6–8	225°
Jackson et al. [2002]	7–10	north of 300°	13–17	210°
Jackson et al. [2002] revised	at least 7	north of 300°	less than 11	210°
Vernant et al. [2004b]	6 ± 2	345°	6.5 ± 2	220°

[a]SCB, South Caspian Basin; EU, Eurasia; and CIB, Central Iranian Block. As estimated by this paper, *Jackson et al.* [2002], the method of *Jackson et al.* [2002] using a revised estimate of the Eurasia-Central Iran motion (*Jackson et al.* [2002] revised), and *Vernant et al.* [2004b].

et al. [2002], in the absence of GPS data, used too high a value. In addition, slightly different assumptions regarding the direction of relative motion of Central Iran and the South Caspian led *Jackson et al.* [2002] to use a direction of 210° compared with the 225° used here, and *Jackson et al.* [2002] did not have the benefit of GPS data for the motion in the eastern Turkish-Iranian Plateau, so had to estimate the direction of South Caspian-Eurasia motion directly. If we recreate the argument used by *Jackson et al.* [2002] using the GPS-based central Iran-Eurasia motion used here, we get estimates of South Caspian-Eurasia motion of at least 7 mm yr^{-1} in a direction north of 300°, and South Caspian-central Iran motion of no more than 11 mm yr^{-1} in the direction 210°.

[26] To summarize, we have estimated the motion of the South Caspian using a construction of velocity triangles. Although our estimate for the motion of the South Caspian does not agree with the suggestion of *Vernant et al.* [2004b], it is consistent with the deformation occurring in the Alborz mountains suggested by *Vernant et al.* [2004b] and also with the deformation which appears to be taking place at the boundary between the South Caspian and the eastern margin of the Turkish-Iranian Plateau.

4. Age of the Present Faulting Configuration

[27] A summary of how the present-day faulting is related to the overall velocity field and the motions of identifiably rigid blocks is given in Figure 13. An important question to then address is for how long this faulting has been active in its present configuration and kinematic pattern. In the absence of direct dating information on most of the faults, one way of approaching this problem is to ask how long it would take to achieve the observable offsets on these faults, if they were always active at present-day rates. That is the purpose of this section.

4.1. Turkish-Iranian Plateau

[28] Total offsets on faults in the Turkish-Iranian Plateau can be estimated through observations of offset geomorphological features, restoration of pull-apart basins, and examination of geological maps, as described below. The relevant information on offsets, slip rates and inferred duration of movement are summarized in Table 3. Throughout this section we have calculated the apparent age of initiation of faults in the Turkish-Iranian Plateau by assuming that slip rates have remained constant through time. Some authors have suggested [e.g., *Friedrich et al.,* 2003] that the slip rates of faults may vary with time, and this may be one reason for the debate surrounding the slip rate and offset of the Main Recent Fault (section 4.3). However, some studies have also suggested that the short- and long-term slip rates on faults are the same. For instance, *Reilinger et al.* [2006] compare current slip rates (from GPS) with longer-term slip rates for a number of faults in the Mediterranean and middle east and find that with the exception of the faults in the Zagros and the Gulf of Corinth, current and long-term slip rates are (within error) in agreement. *England and Molnar* [2005] showed that the strain rate field in Asia constructed using GPS observations is consistent with geological observations of the Quaternary slip rate on faults. *Van Der Woerd et al.* [2000] and *Colgan* [2004] document constant slip rates for major intracontinental faults on timescales of tens of thousands to tens of millions of years, respectively. In the absence of any conclusive evidence regarding fault slip rate constancy (which may not necessarily be the same for all faults), we have assumed, as the simplest alternative, that the slip rates on the faults we study here have remained constant through time. It should be emphasized, however, that the conclusions regarding the age of initiation of faulting rely entirely on this assumption. The estimates of total displacement on the faults are made using a variety of observations. On some faults, rivers entrenched into deep gorges provide "piercing points" which can be used estimate the total offset. In other situations the "closure" of pull-apart basins has been used. We are encouraged in this by observations from the Gailatu-Siah Chesmeh-Khoy fault, and other similar tectonic features elsewhere [e.g., *Walker and Jackson*, 2002] which suggest that the offset estimated from river restorations agrees with the amount of motion required to bring the bedrock on pull-apart margins into contact. However, these estimates are likely to be less accurate that those involving river reconstructions.

4.1.1. Gailatu-Siah Chesmeh-Khoy Fault

[29] Figure 14 shows the Gailatu-Siah Chesmeh-Khoy fault before and after restoration of 13 km of right-lateral strike-slip motion. This restoration closes the Siah-Chesmeh pull-apart basin which is shown shaded gray, and straightens the courses of two large rivers (shown by solid white lines) across the fault. We suggested in section 3.3 that the Gailatu-Siah Chesmeh-Khoy fault and the Pambak-Sevan-Sunik fault are both part of the same array of rotating faults.

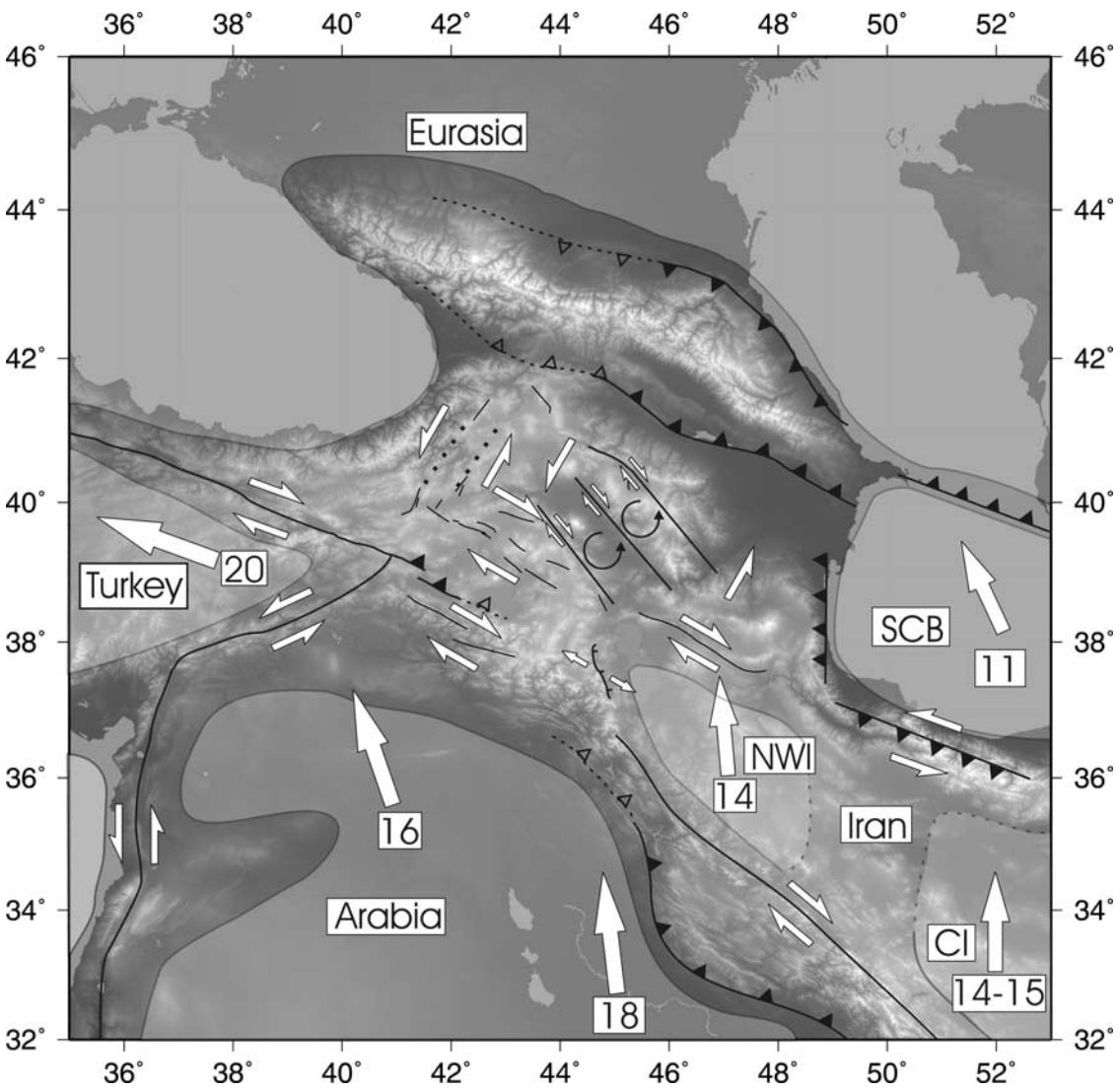

Figure 13. Summary of the active tectonics of the Turkish-Iranian Plateau. Dotted lines east of the Black Sea indicate that the precise locations of the left-lateral faults are not known. Dashed lines with open triangles show where the amount of motion on thrust faults is dying out. The uniformly shaded areas of Turkey, Arabia, Central Iran (CI), NW Iran (NWI), the South Caspian Basin (SCB), and Eurasia are relatively undeforming, based on seismological, GPS and topographic information. The white arrows and associated numbers represent the motion of these undeforming areas with respect to Eurasia (in mm yr^{-1}). The motion of Arabia with respect to Eurasia was calculated using the Euler pole of *McClusky et al.* [2003].

Table 3. Inferred Ages of Faults Within the Turkish-Iranian Plateau[a]

Name of Fault	Offset, km	Slip Rate, mm yr^{-1}	Age, Ma
Gailatu-Siah Chesmeh-Khoy fault	13	2–4	3.5–6.5
Pambak-Sevan-Sunik fault	12	2–4	3–6
South Van faults	9	2–3	3–4.5
Chaldiran and Ercis faults	12.3	8	1.5
Serow normal faults	9	1.5–3.0	3.0–6.0

[a]Deduced using measured offsets and estimates of slip rates. See text for details.

We therefore assume that the slip rate of the Gailatu-Siah Chesmeh-Khoy fault is the same as that measured on the Pambak-Sevan-Sunik fault (see below), which along with the offset of 13 km suggests an age of initiation of the faulting of 3.5–6.5 Ma.

4.1.2. Pambak-Sevan-Sunik Fault

[30] Figure 15 shows part of the Pambak-Sevan-Sunik fault before and after restoration of 12 km of motion. This restoration straightens the course of the large river (the solid white line) across the fault. The offset of 12 km is similar to the estimate of *Philip et al.* [2001], who suggest a minimum offset of 8 km based on the rearranged river courses on the

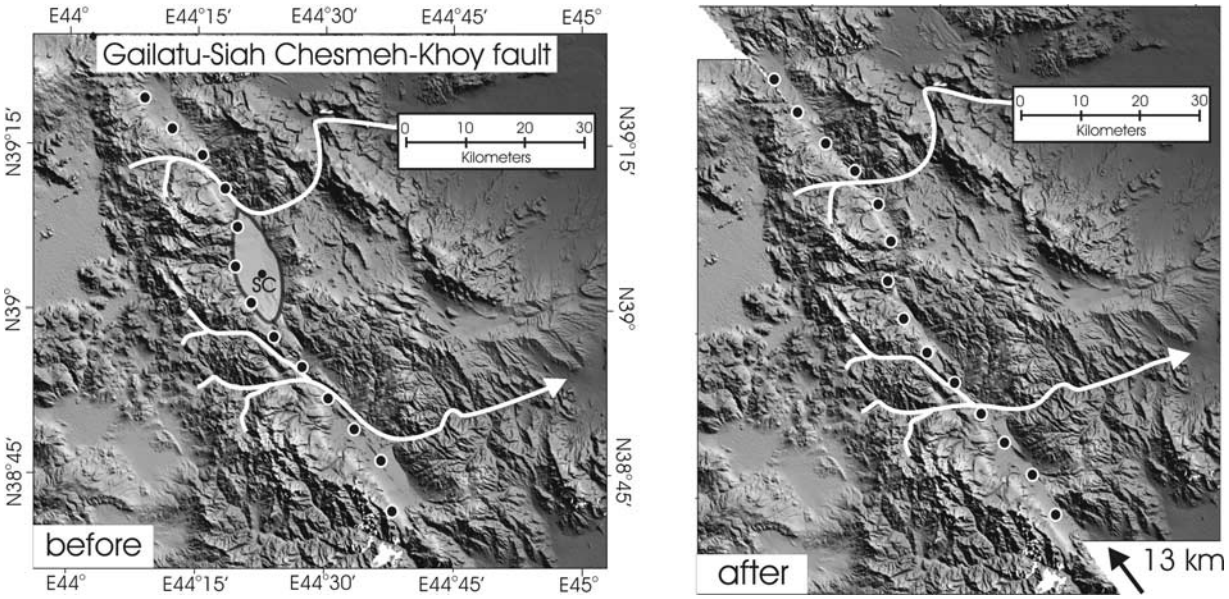

Figure 14. Shaded topographic image of the Gailatu-Siah Chesmeh-Khoy fault before and after restoration of 13 km of motion. The location of the fault is shown by the dotted black line. Removing 13 km of right-lateral motion along the fault straightens the courses of the two large rivers at the fault, shown by the solid white lines, and closes the pull-apart basin at Siah Chesmeh (SC) which is shown shaded in gray on the "before" image.

northern side of the fault at the river valley marked A. *Trifonov et al.* [1994] and *Philip et al.* [2001] have studied the slip rate of this fault using offset rivers and paleoseismology, and the rates generally fall between 2 and 4 mm yr^{-1}. At these rates, a duration of between 3 and 6 Ma is necessary to produce the inferred offsets.

4.1.3. Ercis and Chaldiran Faults

[31] These faults are both right-lateral strike slip in nature, are subparallel, and are only 30 km apart, so will be considered together. Figure 16 shows the Ercis fault before and after the restoration of 11 km of motion. This restores the line of the range front at the location marked A,

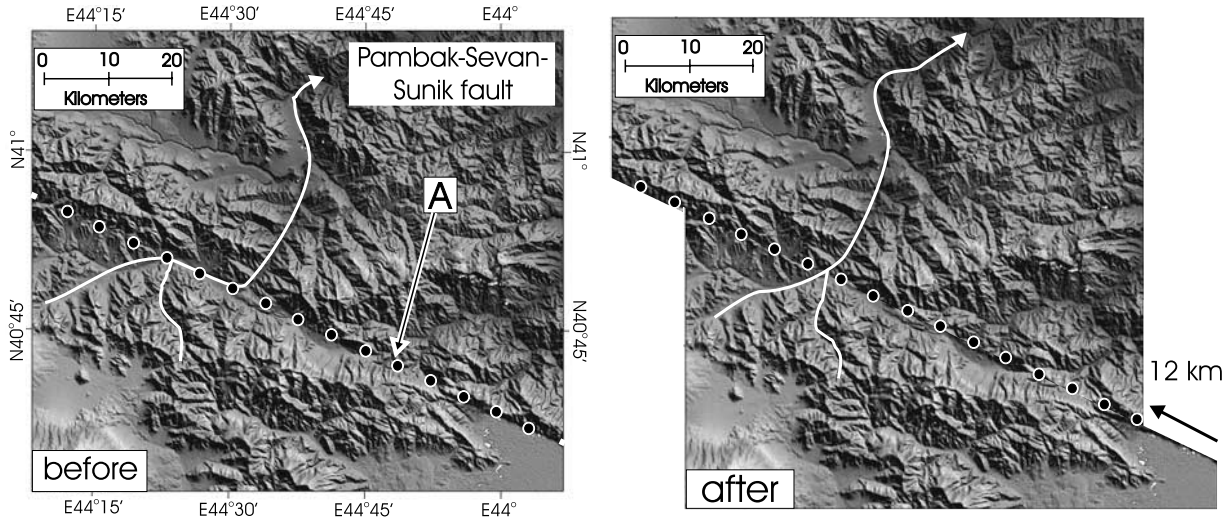

Figure 15. Shaded topographic image of the Pambak-Sevan-Sunik fault before and after restoration of 12 km of motion. The location of the fault is shown by the dotted black line. Removing 12 km of right-lateral motion straightens the course of a river crossing the fault, shown by the solid white line. *Philip et al.* [2001] suggest a minimum total displacement of 8 km based on abandoned river courses at the location marked A in the "before" image.

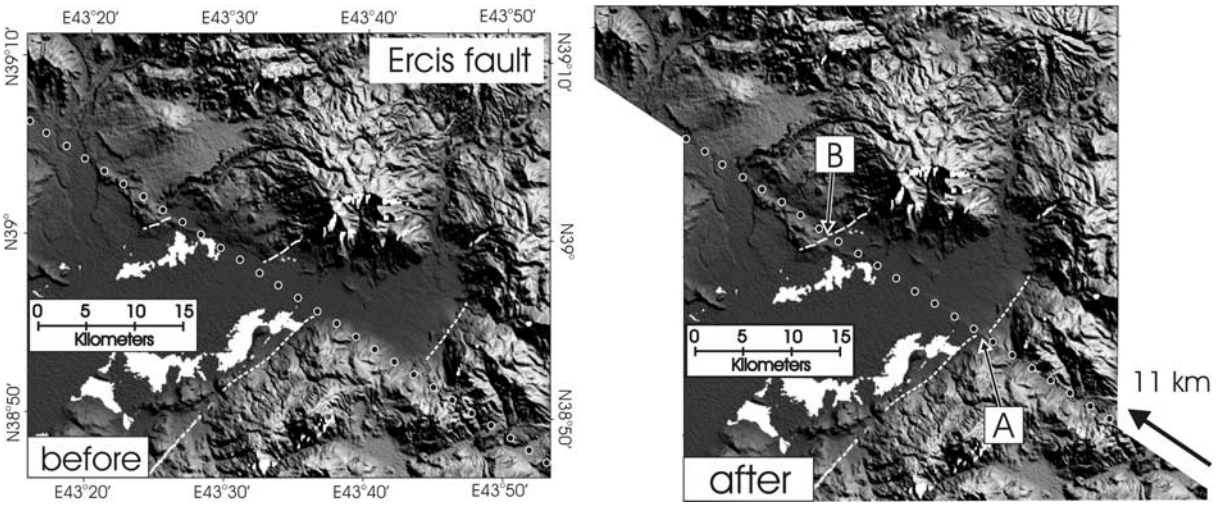

Figure 16. Shaded topographic image of the Ercis fault before and after restoration of 11 km of motion. Removing 11 km of right-lateral motion along the line of the fault (the dotted white line) restores the line of the range front at the location marked A and the edge of volcanic rocks at the location marked B (both shown by dashed white lines). The white areas are "holes" in the SRTM digital elevation model caused by missing data.

and the edge of volcanic rocks visible on satellite pictures at the location marked B (both shown by dashed white lines). We treat these features as piercing points where they meet the fault, although syntectonic erosion may result in (relatively minor) errors in offset estimation. Figure 17 shows the Chaldiran fault before and after the restoration of 1.3 km of motion. This movement restores the axisymmetric shape of the stratovolcano through which the fault passes. It should be noted that the precise age of the volcanic edifice is unknown, so this value represents a minimum offset, as some slip may have occurred before the construction of the stratovolcano. GPS measurements (Figure 4a) show that the combined slip rate for these faults is about 8 mm yr^{-1}, at which rate a duration of approximately 1.5 Ma is needed to account for the combined 12.3 km offset.

4.1.4. South Van Fault

[32] Figure 18 shows two parts of the South Van fault. Figure 18a shows a pull-apart basin (shaded in gray) produced by a change in strike of the fault. The amount of movement required to close the pull-apart basin suggests a total offset on the fault of 9 km. Figure 18b shows a river course (white lines) which has been offset between the locations marked A and B. The size of this offset (9 km) is the same as the amount of motion required to close the pull-apart basin in Figure 18a. GPS measurements (Figure 4a) show that the velocity difference across the area occupied

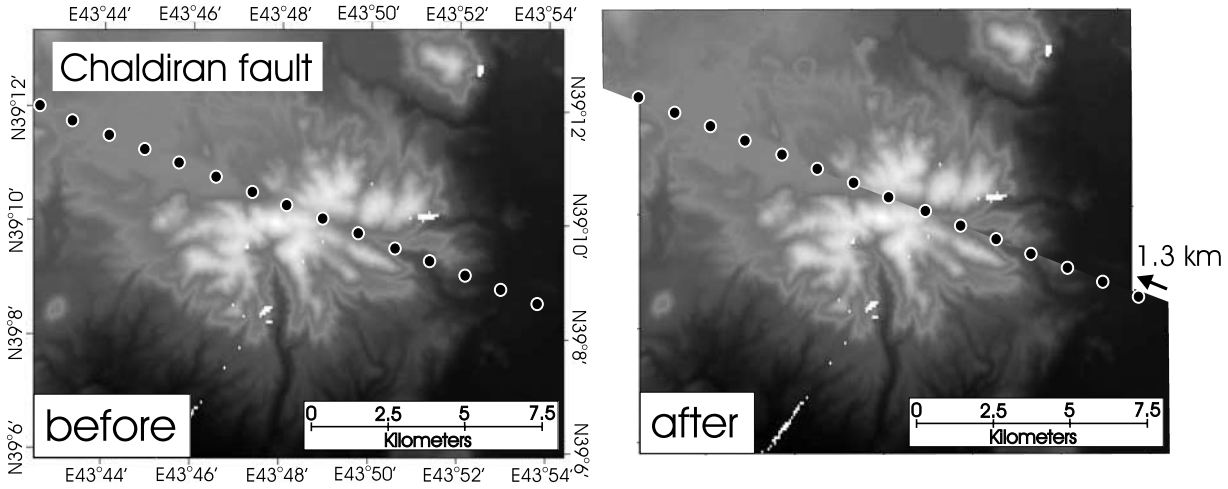

Figure 17. Topographic image of part of the Chaldiran fault before and after restoration of 1.3 km of motion. This motion restores the axisymmetric shape of the high stratovolcano (light colored) in the image.

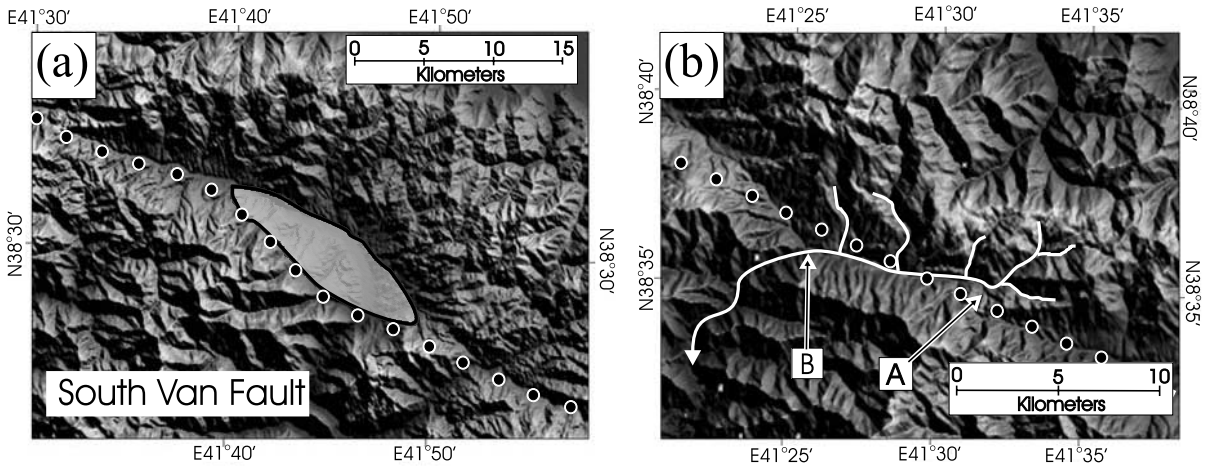

Figure 18. Shaded topographic images for two parts of the South Van fault (the dotted white line). (a) A pull-apart basin (shaded in gray), produced by a change in strike of the fault, can be closed by a total offset on the fault of 9 km. (b) A river course (white lines) which has been offset between the locations marked A and B. The size of this offset (9 km) is the same as the amount of motion required to close the pull-apart basin in Figure 18a.

by the South Van fault is 2–3 mm yr^{-1}, at which rate a duration of 3–4.5 Ma is needed to account for the offset.

4.1.5. Serow Normal Faults

[33] The offset of a thin (500 m) steeply dipping band of Eocene conglomerates can be used to estimate a total horizontal offset. The precise dip of this conglomerate band is unknown, but we know the dip to be steep [*Geological Survey of Iran*, 1976] and assume for the purposes of this estimation that the dip is vertical. In this case, the total offset will be given by the offset parallel to the slip vector (section 2.2). We estimate this offset to be 9 km parallel to the slip vector direction of 290°–300° (Figure 19). In section 3.1 we suggested that these faults have a horizontal slip rate of approximately 1.5–3.0 mm yr^{-1}. These rates would require 3–6 Ma to account for the 9 km offset.

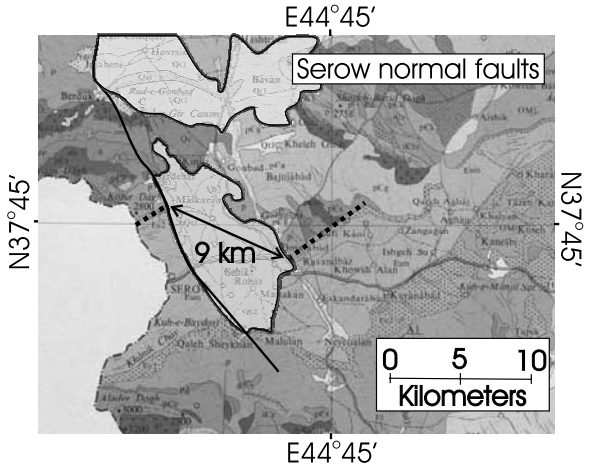

Figure 19. Detail from a 1:250,000 scale geological map of part of the Serow normal faults (adapted from *Geological Survey of Iran* [1976]). The NW-SE black line marks the fault. The arrowed black line shows an offset of a thin (500 m wide) band of steeply dipping Eocene conglomerates (the dotted lines) of 9 km parallel to the slip vector measured on the exposed fault plane in Figure 5a. The gray shaded areas (outlined in black) show the approximate extent of the Quaternary sediments in the hanging wall basin. The areas are separated from each other by Quaternary volcanic rocks.

4.2. North and East Anatolian Faults

[34] *Armijo et al.* [1999] conclude that slip at the western end of the North Anatolian Fault started at around 5 Ma or younger based on the offset of an unconformable marine transgression following the Mediterranean Messinian crisis. Ages of up to 13 Ma have been suggested for the onset of slip at the eastern end of the fault [*Hubert-Ferrari et al.*, 2002, and references therein], but these rely on the dating of sediments in basins along the fault, which may predate the faulting. The total offset on the North Anatolian Fault is thought to be around 80 to 85 km [*Westaway*, 1994; *Armijo et al.*, 1999; *Hubert-Ferrari et al.*, 2002]. The Holocene slip rate for the fault has been estimated to be 18 ± 3.5 mm yr^{-1} based on offset features of presumed Holocene deglaciation age, 18 ± 5 mm yr^{-1} from ^{14}C dating of offset river terraces [*Hubert-Ferrari et al.*, 2002], and ~22 mm/yr from cosmogenic chlorine 18 dating, also of river terraces [*Kozaci et al.*, 2004]. The slip rate determined by GPS has a lower limit of 20 ± 3 mm yr^{-1} based on dense measurements in the Mamara region, and an upper limit of 24 ± 1 mm yr^{-1} based on the Euler pole for Anatolia-Eurasia motion derived from the GPS measurements [*McClusky et al.*, 2000]. Extrapolation of the GPS and Holocene rates would achieve the total offset between 3.3 Ma (using the geodetically deduced rate of 24 mm yr^{-1} and a total offset of 80 km) and 4.7 Ma (using the Holocene rate of 18 mm yr^{-1} and a total offset of 85 km).

[35] The onset of motion on the East Anatolian Fault is thought to be at around 3 Ma or younger [*Saroglu et al.*, 1992b; *Westaway and Arger*, 1996] based on geological offsets and kinematic models. *Westaway and Arger* [2001], however, show that another fault zone, west of the East Anatolian Fault but also connecting the Dead Sea fault zone and the North Anatolian Fault, was active between 3 and 5 Ma and accumulated 29 km of displacement. Therefore, although slip on the East Anatolian Fault may date from only 3 Ma, left-lateral faulting had been taking place in this area since around 5 Ma. A third major strike-slip fault emanating from the Turkish-Iranian Plateau is the Main Recent Fault, which is discussed in detail below.

4.3. Main Recent Fault

[36] The two pull-apart basins described in section 2.6 and shown in Figure 7 give an estimate of the total displacement at the NW end of the Main Recent Fault of 10–15 km. Farther SE, *Talebian and Jackson* [2002] estimated the total displacement, using offset drainage patterns and geological evidence, to be 50 km. Taken together, these two different estimates of displacement require either (1) that there must be a significant gradient in total displacement and slip rate along the fault, (2) that the fault is older in the area studied by *Talebian and Jackson* [2002] than at the northwestern end, if the slip rate is constant along the whole fault, or (3) that one or both of the estimates of total displacement is wrong.

[37] There are no obvious structures along the Main Recent Fault, in the form of normal or thrust faults at a high angle to its strike, which would allow for the accommodation of the 35–40 km difference in total displacement that is required if both estimates of total offset are correct. This suggests that either the onset of faulting was diachronous along the length of the Main Recent Fault, or that one of the estimates of offset is in error.

[38] *Talebian and Jackson* [2002] argued that the age of the Main Recent Fault in the area they studied (~33°N 49°E) was probably 3–5 Ma, because that was the time of onset of shortening in the Simple Folded Zone of the Zagros [*Falcon*, 1974], and the role of the Main Recent Fault seems to be to take up oblique shortening by strain partitioning. *Authemayou et al.* [2006] suggest a similar age of late Pliocene in the same region based on faults and folds of this age which are cut by the Main Recent Fault. If the slip rate on the fault has been constant through time, then an age of 3–5 Ma is equivalent to a slip rate of 10–17 mm yr^{-1} if the total displacement is 50 km, or 2–5 mm yr^{-1} if the total displacement is 10–15 km. Geodetic estimates for the slip rate on the Main Recent Fault are 3 ± 2 mm yr^{-1} from the sparse national GPS network [*Vernant et al.*, 2004a] and 4–6 mm yr^{-1} from a denser local network [*Walpersdorf et al.*, 2006]. *Authemayou* [2006] suggests a quaternary slip rate of 5–7 mm yr^{-1} from cosmogenic dating of offset features. If the modern slip rate has been constant for 3–5 Ma, then the offset of 10–15 km is likely to be accurate. If, however, the slip rate was higher in the past than it is today, then the offset of 50 km may be correct, and either the offset of 10–15 km is in error, or the onset of faulting was later near the NW end of the Main Recent Fault than in the area farther SE studied by *Talebian and Jackson* [2002]. We do not know which of these possibilities is more likely.

4.4. Summary

[39] Offsets on the Serow normal faults, the Gailatu-Siah Chesmeh-Khoy fault, the Pambak-Sevan-Sunik fault, and the South Van fault (Table 3) all suggest that if slip rates have been constant throughout the duration of faulting, the faults started moving 5 ± 2 Myr ago. However, the Chaldiran and Ercis faults need only 1.5 Ma to produce their apparent offsets at present-day rates and, by this argument, appear to be younger (although one of the offsets used in this calculation is only a minimum offset, and may not represent the total offset). In addition, the major strike-slip systems emanating from the plateau also appear to have begun accumulating significant displacement at around 5 ± 2 Ma.

5. Discussion

[40] The principal aim of this work was to understand how the present-day faulting in the Turkish-Iranian Plateau accommodates the Arabia-Eurasia motion and the deforming velocity field revealed by GPS measurements. By estimating the offsets on faults within the plateau we have also been able to show that the present-day kinematics, operating at present-day rates, can account for those offsets in about 5 ± 2 Ma. Two remaining questions need comment. First, why is the strike-slip faulting so complicated in the plateau region, but simple to either side? Secondly, what happened at 5 ± 2 Ma to change the fault pattern, since the onset of Arabia-Eurasia collision certainly predated that time?

5.1. Distributed Nature of the Strike-Slip Faulting

[41] Right-lateral strike-slip faulting within the Turkish-Iranian Plateau is distributed, while that to the east and west of the plateau it is localized onto individual faults (the North Anatolian and Main Recent faults, respectively). We see two main reasons why this difference in the nature of the faulting may have occurred. First, the North Anatolian and Main Recent faults follow geological suture zones (the IntraPontide Suture and the Main Zagros Reverse Fault [e.g., *Hubert-Ferrari et al.*, 2002; *Talebian and Jackson*, 2002, and references therein]. The Pontide Suture curves northward from its position south of the Black Sea as it enters the Turkish-Iranian Plateau (Figure 3) and crosses the Plateau north of the distributed strike-slip faulting, while the Bitlis Suture runs along the very southern edge of the plateau, south of the distributed strike-slip faulting [*Sengör and Yilmaz*, 1981]. Therefore there are no suture zones near the distributed strike-slip faulting of the Van Shear Zone in the central parts of the Turkish-Iranian Plateau. If suture zones represent inherited weak areas of crust which serve to localize deformation, then an absence of suture zones, and so preexisting strength contrasts, may explain why the strike-slip faulting on the plateau is distributed, while in areas with

suture zones the faulting is more localized. Secondly, there is active shortening in the Greater Caucasus, north of the distributed strike-slip faulting, which has the affect of advecting material in the plateau northeastward [*Jackson*, 1992]. In the 5 ± 2 Ma in which the faulting has been present in its current configuration the faults would be expected to have moved NE by 18–63 km relative to the North Anatolian Fault. This distance is similar to, or smaller than, the width of the Van shear zone. NE movement of the strike-slip faults may prevent the survival of a continuous throughgoing fault from the North Anatolian Fault to the Main Recent Fault. We do not know the relative importance of these two possibilities.

5.2. Change in the Nature of the Collision Zone at 5 ± 2 Ma

[42] The available evidence suggests that the faulting within the Turkish-Iranian Plateau has been present in its current configuration since 5 ± 2 Ma. Radiometric dating of volcanic rocks [e.g., *Innocenti et al.*, 1976a, 1976b; *Pearce et al.*, 1990] suggests the onset of major volcanism in the plateau at 6–8 Ma. *Morton et al.* [2003] have studied the provenance of sediment supply to the South Caspian Basin, and have found that above the base of the Productive Series, which began deposition at around 5.5 Ma, there is increased influx of sand derived from the Greater Caucasus, which is presumably related to increased erosion, which may suggest increased topography and uplift rates. The apatite fission track data of *Kral and Gurbanov* [1996] show an increase in exhumation in the eastern Greater Caucasus at 7–4 Ma. *Khain and Milanovsky* [1963], quoted by *Philip et al.* [1989], note that the transition from a marine to continental environment and the onset of deposition of coarse clastics in part of the basins on the southern flank of the eastern Greater Caucasus began at 5 Ma. *Axen et al.* [2001] documented increased exhumation rates in the west central Alborz after 7 Ma. These all suggest a significant change in the nature of the collision zone at 5 ± 2 Ma, as was also noted by *Allen et al.* [2004]. *Allen et al.* [2004] attribute this change to crustal thickening migrating away from the interior of the Turkish-Iranian Plateau, which was at sea level in the Miocene and is now ~2 km high, toward the surrounding lowlands. This is the expected mode of growth for a plateau as buoyancy forces concentrate near the gradients in crustal thickness [e.g., *England and Houseman*, 1988].

[43] Recently published results shed further light on the deep structure of the Turkish-Iranian Plateau. *Zor et al.* [2003] used seismic receiver functions to estimate the crustal thickness of the SW part of the plateau. They found values between 40 and 50 km, suggesting that most of the southwestern part of the plateau is isostatically undercompensated at the Moho and must be dynamically supported in the mantle [e.g., *Sengör et al.*, 2003]. *Maggi and Priestley* [2005] used higher-mode surface wave tomography to demonstrate an area of low velocity in the upper mantle to depths of around 200 km beneath the plateau, in the same location as a long-wavelength positive free-air gravity anomaly [*Lemoine et al.*, 1996]. These results all suggest that the elevation of the Turkish-Iranian Plateau is at least in part supported by density variations in the mantle rather than by isostatic compensation of thick crust.

[44] Thus the suggestion of *Allen et al.* [2004] that the change in the nature of the faulting within the collision zone was a response to uplift of the plateau and a migration of deformation to its edges may be correct. However, in the light of the new information regarding the nature of the plateau at depth, it is more probable that this uplift was due to a dynamically supported increase in elevation rather than crustal thickening. The low-density, and therefore presumably hot, material in the upper mantle below the plateau that is responsible for this increase in elevation is the likely cause of major volcanism on the plateau, which was roughly coincident with the onset of the current configuration of faulting.

[45] The nature of the area of low-density material in the upper mantle below the Turkish-Iranian Plateau is unknown. On the basis of the chemistry of volcanic rocks in the area *Pearce et al.* [1990] attribute the volcanic activity either to lower lithosphere delamination or a deep-seated mantle plume, but there is little evidence for either in the seismic tomography of *Maggi and Priestley* [2005]. Nonetheless, something seems to have occurred that led to a change in upper mantle temperature structure between the onset of continental shortening at about 12 Ma [*Dewey et al.*, 1986; *McQuarrie et al.*, 2003], and the change in the nature of the collision zone at about 5 Ma.

6. Conclusions

[46] Enough is now known of the geometry and kinematics of the faulting in the Turkey-Iran-Caucasus collision zone to see how it accommodates the deforming velocity field observed by GPS. The principal results in this regard are as follows:

[47] 1. The right-lateral strike-slip faulting of the Turkish-Iranian Plateau is most active (8 ± 2 mm yr^{-1}) in a WNW-ENE band near Lake Van.

[48] 2. Another zone of right-lateral strike-slip faulting in the NE plateau has a NW-SE strike, slower slip rates (2–4 mm yr^{-1}), and rotates counterclockwise relative to Eurasia to accommodate a NW-SE gradient in NE directed velocity.

[49] 3. The origin of this velocity gradient is a combination of the southeastward increasing amount of shortening in the Greater Caucasus, and a southern zone of shortening between the Karliova triple junction and Lake Van which dies out to the east.

[50] 4. A band of oblique normal faults running NNW-SSE along the Turkey-Iran border is probably related to either rapid changes in orientation and rate of overall Arabia-Eurasia motion close to the Euler pole, or to the NW end of the Main Recent Fault, or both.

[51] By estimating the offsets on faults, mostly from displaced geomorphological features, we show that those offsets can be achieved in 5 ± 2 Ma, at present rates. This is consistent with a reorganization of the deforming zone at that time, and therefore after the initial collision at ~12 Ma,

as various authors have suggested from other observations elsewhere. It is probable that the reorganization is a response to uplift associated with density anomalies in the mantle, though the origin of these anomalies is unclear.

[52] **Acknowledgments.** We thank J. Hollingsworth and M. Talebian for assistance in the field and M. Korehie and M. Ghorashi of the Geological Survey of Iran for continued support of our work over several years. We are grateful to R. Reilinger, C. Authemayou, and A. Walpersdorf for giving us access to their work before publication. We wish to thank Brian Wernicke and Robert Reilinger for helpful and constructive reviews. This work is supported by a NERC grant to COMET (http://comet.nerc.ac.uk). Some figures were produced using the Generic Mapping Tools (GMT) software [*Wessel and Smith*, 1995].

References

Allen, M., M. R. Ghassemi, M. Shahrabi, and M. Qorashi (2003), Accomodation of late Cenozoic oblique shortening in the Alborz range, northern Iran, *J. Struct. Geol.*, *25*, 659–672.

Allen, M., J. Jackson, and R. Walker (2004), Late Cenozoic reorganization of the Arabia-Eurasia collision and the comparison of short-term and long-term deformation rates, *Tectonics*, *23*, TC2008, doi:10.1029/2003TC001530.

Ambraseys, N. N. (1988), Engineering seismology, *Earthquake Eng. Struct. Dyn.*, *17*, 1–105.

Ambraseys, N. N., and A. Zátopek (1968), The Varto Üstükran (Anatolia) earthquake of 19 August 1966, summary of a field report, *Bull. Seismol. Soc. Am.*, *58*, 47–102.

Armijo, R., B. Meyer, A. Hubert, and A. Barka (1999), Westward propagation of the North Anatolian fault into the northern Aegean: Timing and kinematics, *Geology*, *27*, 267–270.

Authemayou, C. (2006), Partitionment de la convergence oblique en zone de collision: Example de la chaine du Zagros (Iran), Ph.D. thesis, Univ. Paul Cezanne Aix-Marseille III, Aix-Marseille, France.

Authemayou, C., D. Chardon, O. Bellier, Z. Malekzadeh, E. Shabanian, and M. R. Abbassi (2006), Late Cenozoic partitioning of oblique plate convergence in the Zagros fold-and-thrust belt (Iran), *Tectonics*, *25*, TC3002, doi:10.1029/2005TC001860.

Axen, G. J., P. S. Lam, M. Grove, D. F. Stockli, and J. Hassanzadeh (2001), Exhumation of the west-central Alborz Mountains, Iran, Caspian subsidence, and collision-related tectonics, *Geology*, *29*, 559–562.

Barka, A. A., and K. Kadinsky-Cade (1988), Strike-slip fault geometry in Turkey and its influence in earthquake activity, *Tectonics*, *7*, 663–684.

Barka, A., I. Kuscu, and H. Kato (1985), Horasan-Narman (Erzerum, Turkey) earthquake of 30th October, 1983, *ITIT Project 8212*, pp. 70–83, Geol. Surv. of Jpn., Tsukuba.

Berberian, M. (1997), Seismic sources of the Transcaucasian historical earthquakes, in *Historical and Prehistorical Earthquakes in the Caucasus*, edited by D. Giardini and S. Balassanian, pp. 233–311, Springer, New York.

Berberian, M., and J. S. Tchalenko (1976), Field study and documentation of the 1930 Salmas (Shahpur-Azarbaidjan) earthquake, in *Contribution to the Seismotectonics of Iran, part II*, edited by M. Berberian, *Rep. 39*, pp. 271–342, Geol. Surv. of Iran, Tehran.

Bozkurt, E. (2001), Neotectonics of Turkey—A synthesis, *Geodin. Acta*, *14*, 3–30.

Colgan, J. (2004), Estimating normal fault slip rates over a ten million-year interval using apatite fission track and (U-Th)/He thermochronology, *Geol. Soc. Am. Abstr. Programs*, *36*, 427.

Dewey, J. F., M. R. Hempton, W. S. F. Kidd, F. Saroglu, and A. M. C. Şengör (1986), Shortening of continental lithosphere: The tectonics of eastern Anatolia—A young collision zone, *Geol. Soc. Spec. Publ.*, *19*, 3–36.

Engdahl, E., R. van der Hilst, and R. Buland (1998), Global teleseismic earthquake relocation with improved travel times and procedures for depth determination, *Bull. Seismol. Soc. Am.*, *88*, 722–743.

England, P., and G. Houseman (1988), The mechanics of the Tibetan Plateau, *Philos. Trans. R. Soc. London.*, *326*, 301–320.

England, P., and P. Molnar (2005), Late Quaternary to decadal velocity fields in Asia, *J. Geophys. Res.*, *110*, B12401, doi:10.1029/2004JB003541.

Falcon, N. L. (1974), Southern Iran: Zagros Mountains, in *Mesozoic-Cenozoic Orogenic Belts, Data for Orogenic Studies*, edited by A. M. Spencer, *Geol. Soc. Spec. Publ.*, *4*, 199–211.

Friedrich, A. M., B. P. Wernicke, N. A. Niemi, R. A. Bennett, and J. L. Davis (2003), Comparison of geodetic and geologic data from the Wasatch region, Utah, and implications for the spectral character of Earth deformation at periods of 10 to 10 million years, *J. Geophys. Res.*, *108*(B4), 2199, doi:10.1029/2001JB000682.

Fuenzalida, H., et al. (1997), Seismic source study of the Racha-Dzhava (Georgia) earthquake from aftershocks and broad-band teleseismic body-wave records: An example of active nappe tectonics, *Geophys. J. Int.*, *130*, 29–46.

Geological Survey of Iran (1976). Serow quadrangle map, Tehran.

Guidoboni, E., R. Haroutiunian, and A. Karakhanian (2003), The Garni (Armenia) large earthquake on 14 June 1679: A new analysis, *J. Seismol.*, *7*, 301–328.

Hubert-Ferrari, A., R. Armijo, G. King, B. Meyer, and A. Barka (2002), Morphology, displacement, and slip rates along the North Anatolian Fault, Turkey, *J. Geophys. Res.*, *107*(B10), 2235, doi:10.1029/2001JB000393.

Innocenti, F., R. Mazzuoli, G. Pasquare, F. Radicati di Brozolo, and L. Villari (1976a), Evolution of volcanism in the area of interaction between the Arabian, Anatolian and Iranian plates (Lake Van, Eastern Turkey), *J. Volcanol. Geotherm. Res.*, *1*, 103–112.

Innocenti, F., R. Mazzuoli, G. Pasquare, F. Radicati di Brozolo, and L. Villari (1976b), Tertiary and Qaternary volcanism in the Erzerum-Kars area (eastern Turkey): Geochronological data and geodynamic evolution, *J. Volcanol. Geotherm. Res.*, *13*, 223–240.

Jackson, J. (1992), Partitioning of strike-slip and convergent motion between Eurasia and Arabia in eastern Turkey and the Caucasus, *J. Geophys. Res.*, *97*, 12,471–12,479.

Jackson, J., K. Priestly, M. Allen, and M. Berberian (2002), Active tectonics of the South Caspian Basin, *Geophys. J. Int.*, *148*, 214–245.

Karakhanian, A. (1993), The active faults of the Armenian Upland, paper presented at Scientific Meeting on Seismic Protection, Venice, Italy.

Karakhanian, A. S., R. A. Arutiunian, and N. A. Babayan (1993), Map of active faults and seismotectonics of the territory of the Armenian Upland, Natl. Surv. for Seismic Protect, Yerevan, Armenia.

Karakhanian, A. S., et al. (2004), Active faulting and natural hazards in Armenia, eastern Turkey and northwest Iran, *Tectonophysics*, *380*, 189–219.

Khain, V. E., and E. E. Milanovsky (1963), Structure tectonique du Caucase d'apres les donnees modernes, in *Volume in Honor of Prof. Paul Fallot*, *Mem. Soc. Geol. Fr.*, *1*, 663–703.

Kozaci, O., J. Dolan, R. Finkel, R. Hartleb, K. Frankel, and A. Hubert-Ferrari (2004), A long-term slip-rate study along the North Anatolian Fault, Eksik, Turkey using cosmogenic ^{36}Cl, *Eos Trans. AGU*, *85*(47), Fall Meet. Suppl., Abstract T41F-1292.

Kral, J., and A. G. Gurbanov (1996), Apatite fission track data from the Great Caucasus pre-Alpine basement, *Chem. Erde*, *56*, 177–192.

Lemoine, F., et al. (1996), The NASA and DMA joint geopotential model, *Eos Trans. AGU*, *77*(46), Fall Meet. Suppl., F136.

Maggi, A., and K. Priestley (2005), Surface waveform tomography of the Turkish-Iranian plateau, *Geophys. J. Int.*, *160*, 1068–1080.

McClusky, S., et al. (2000), Global Positioning System constraints on plate kinematics and dynamics in the eastern Mediterranean and Caucasus, *J. Geophys. Res.*, *105*, 5695–5719.

McClusky, S., R. Reilinger, S. Mahmoud, D. Ben Sari, and A. Tealeb (2003), GPS constraints on Africa (Nubia) and Arabia plate motions, *Geophys. J. Int.*, *155*, 126–138.

McKenzie, D. (1970), Plate tectonics of the Mediterranean region, *Nature*, *226*, 239–243.

McKenzie, D. (1972), Active tectonics of the Mediterranean region, *Geophys. J.R. Astron. Soc.*, *30*, 109–185.

McQuarrie, N., J. M. Stock, C. Verdel, and B. P. Wernicke (2003), Cenozoic evolution of Neotethys and implications for the causes of plate motions, *Geophys. Res. Lett.*, *30*(20), 2036, doi:10.1029/2003GL017992.

Morton, A., M. Allen, M. Simmons, F. Spathopoulos, J. Still, D. Hinds, A. Ismail-Zadeh, and S. Kroononberg (2003), Provenance patternes in a neotectonic basin: Pliocene and Quaternary sediment supply to the South Caspian, *Basin Res.*, *15*, 321–337.

Pacheco, J., C. Estabrook, D. Simpson, and J. Nabalek (1989), Teleseismic body wave analysis of the 1988 Armenian earthquake, *Geophys. Res. Let.*, *16*, 1425–1428.

Pearce, J. A., et al. (1990), Genesis of collision volcanism in eastern Anatolia, Turkey, *J. Volcanol. Geotherm. Res.*, *44*, 189–229.

Philip, H., A. Cisternas, A. Gvishiani, and A. Gorshkov (1989), The caucassus: An actual example of the initial stages of continental collision, *Tectonophysics*, *161*, 1–21.

Philip, H., A. Avagyan, A. Karakhanian, J.-F. Ritz, and S. Rebai (2001), Estimating slip rates and recurrence intervals for strong earthquakes along an intracontinental fault: Example of the Pambak-Sevan-Sunik fault (Armenia), *Tectonophysics*, *343*, 205–232.

Priestley, K., C. Baker, and J. Jackson (1994), Implications of earthquake focal mechanism data for the active tectonics of the South Caspian Basin and surrounding regions, *Geophys. J. Int.*, *118*, 111–141.

Reilinger, R., et al. (2006), GPS constraints on continental deformation in the Africa-Arabia-Eurasia continental collision zone and implications for the dynamics of plate interactions, *J. Geophys. Res.*, *111*, B05411, doi:10.1029/2005JB004051.

Saroglu, F., and Y. Guner (1979), The Tutak active fault, its characteristics and relation to the Chaldiran fault (in Turkish), *Yeryuvari Insan*, *4*, 11–14.

Saroglu, F., and M. Hempton (1982), Tectonic and sedimentary character of the Mus-Van Basin, SE Turkey, *Eos Trans. AGU*, *63*(18), 442.

Saroglu, F., O. Emre, and I. Kuscu (1992a), Active fault map of Turkey, General Dir. of Miner. Res. and Explor., Ankara, Turkey.

Saroglu, F., O. Emre, and I. Kuscu (1992b), The East Anatolian Fault of Turkey, *Ann. Tectonicae*, *6*, 125–199.

Sengör, A. M. C. (1990), A new model for the late Palaeozoic-Mesozoic tectonic evolution of Iran and implications for Oman, in *The Geology and Tectonics of the Oman Region*, edited by A. H. F. Robertson, M. P. Searle, and A. C. Ries, *Geol. Soc. Spec. Publ.*, *49*, 797–831.

Sengör, A. M. C., and Y. Yilmaz (1981), Tethyan evolution of Turkey: A plate tectonic approach., *Tectonophysics*, *75*, 181–241.

Sengör, A. M. C., S. Özeren, T. Geņc, and E. Zor (2003), East Anatolian high plateau as a mantle-supported, north-south shortened domal structure, *Geophys. Res. Lett.*, *30*(24), 8045, doi:10.1029/2003GL017858.

Talebian, M., and J. Jackson (2002), Offset on the Main Recent Fault of NW Iran and implications for the late Cenozoic tectonics of the Arabia-Eurasia collision zone, *Geophys. J. Int.*, *150*, 422–439.

Talebian, M., and J. Jackson (2004), A reappraisal of earthquake focal mechanisms and active shortening in the Zagros mountains of Iran, *Geophys. J. Int.*, *156*, 506–526.

Tchalenko, J. S., and M. Berberian (1974), The Salmas (Iran) earthquake of May 6th, 1930, *Ann. Geofis.*, *27*, 151–212.

Toksoz, M. N., E. Arpat, and F. Saroglu (1977), East Anatolian earthquake of 24 November 1976, *Nature*, *270*, 423–425.

Trifonov, V. G., A. S. Karakhanian, and A. J. Kozhurin (1994), Major active faults of the collision area between the Arabian and the Eursian plates., paper presented at the Conference on Continental Collision Zone Earthquakes and Seismic Hazard Reduction, IASPEI/UN Int. Decade for Nat. Disaster Reduct., Yerevan, Armenia.

Van Couvering, J. A., and J. A. Miller (1971), Late Miocene marine and non-marine time scale in Europe, *Nature*, *230*, 559–563.

Van der Woerd, J., F. J. Ryerson, P. Tapponnier, A.-S. Meriaux, Y. Gaudemer, B. Meyer, R. C. Finkel, M. W. Caffee, G. Zhao, and Z. Xu (2000), Uniform slip-rate along the Kunlun Fault: Implications for seismic behaviour and large-scale tectonics, *Geophys. Res. Lett.*, *27*, 2353–2356.

Vernant, P., et al. (2004a), Present-day crustal deformation and plate kinematics in the Middle East constrained by GPS measurements in Iran and northern Oman, *Geophys. J. Int.*, *157*, 381–398.

Vernant, P., et al. (2004b), Deciphering oblique shortening of central Alborz in Iran using geodetic data, *Earth Planet. Sci. Lett.*, *223*, 177–185.

Walker, R., and J. Jackson (2002), Offset and evolution of the Gowk fault, S.E. Iran: A major intra-continental strike-slip system, *J. Struct. Geol.*, *24*, 1677–1698.

Walpersdorf, A., D. Hatzfeld, H. Nankali, F. Tavakoll, F. Nilforoushan, M. Tatar, P. Vernant, J. Chery, and F. Masson (2006), Difference in the GPS deformation pattern of North and Central Zagros (Iran), *Geophys. J. Int*, in press.

Wessel, P., and W. Smith (1995), New version of the Generic Mapping Tools released, *Eos Trans. AGU*, *76*, 329.

Westaway, R. (1994), Present-day kinematics of the Middle East and eastern Mediterranean, *J. Geophys. Res.*, *99*(6), 12,071–12,090.

Westaway, R., and J. Arger (1996), The Golbasi basin, southeastern Turkey: A complex discontinuity in a major strike-slip fault zone, *J. Geol. Soc. London*, *153*, 729–743.

Westaway, R., and J. Arger (2001), Kinematics of the Malatya-Ovacik Fault Zone, *Geodin. Acta*, *14*, 103–131.

Zor, E., E. Sandvol, C. Gürbz, N. Türkelli, D. Seber, and M. Barazangi (2003), The crustal structure of the East Anatolian plateau (Turkey) from receiver functions, *Geophys. Res. Lett.*, *30*(24), 8044, doi:10.1029/2003GL018192.

A. Copley and J. Jackson, Department of Earth Sciences, Bullard Laboratories, University of Cambridge, Madingley Road, Cambridge CB2 3EQ, UK. (acc41@cam.ac.uk)